The Journal of Chemical Physics ARTICLE pubs.aip.org/aip/jcp

Microscopic elasticity from MD. II. Liquid interfaces and lipid membranes

Cite as: J. Chem. Phys. 164, 024111 (2026); doi: 10.1063/5.0303850
Submitted: 24 September 2025 • Accepted: 12 December 2025 •
Published Online: 13 January 2026

Andrew L. Lewis,[1] Benjamin Himberg,[2] Alejandro Torres-Sánchez,[3] and Juan M. Vanegas[4,a)]

AFFILIATIONS

[1] Department of Physics, The University of Vermont, Burlington, Vermont 05405, USA
[2] Materials Science Graduate Program, The University of Vermont, Burlington, Vermont 05405, USA
[3] European Molecular Biology Laboratory, Barcelona, Spain
[4] Department of Biochemistry and Biophysics, Oregon State University, Corvallis, Oregon 97331, USA

[a)] **Author to whom correspondence should be addressed:** vanegasj@oregonstate.edu

ABSTRACT

Lipid membranes not only play critical roles in many cellular functions but are also unique in that they have properties of both fluid and elastic materials. While 2D elasticity theories, such as Canham–Helfrich–Evans, adequately capture the dominant energetics of membrane deformation, a full characterization of the 3D elastic response is necessary to account for the many modes of deformation and the role that lipid structure plays in determining the elastic energy. We use the stress–stress fluctuation (SSF) method to obtain local elasticity profiles of a simple water–dodecane interface and a lipid membrane from coarse-grained MARTINI molecular dynamics simulations. We validate the results from the SSF method through the explicit deformation method, which measures the change in the local stress tensor relative to a specific strain. Furthermore, we show that some expected symmetries of the elasticity tensor are locally broken due to the lateral fluidity of the interfacial systems and the physical constraint of mechanical equilibrium. Profiles of the lateral and transverse shear moduli show that the membrane is locally fluid, while the transverse shear modulus is locally nonzero, but its integral vanishes. We define the area, Young's, and bulk moduli, as well as the Poisson ratio for a lipid membrane through the compliance tensor, and use the area modulus to estimate the position of the neutral surface and the macroscopic bending modulus. Our elasticity calculations provide critical insights into the local mechanical properties of lipid bilayers and unravel the role of lateral fluidity in the membrane's elastic response.

I. INTRODUCTION

The mechanical properties of lipid membranes play a key role in modulating many biological functions, such as membrane fission, fusion, organelle shaping, and cellular remodeling.[1–6] In these processes, the energetics of deformation, e.g., bending or stretching, are determined by factors such as membrane composition, leaflet asymmetry, and the inclusion or association of proteins, among others. The membrane's elastic energy is most commonly treated with the classical Canham–Helfrich–Evans (CHE) theory,[7–9] which assumes a two-dimensional film with no internal structure. Within the CHE theory, the material constants that determine the elastic energy of the sheet are the bending, κ, and Gaussian curvature, $\bar{\kappa}$, moduli, as well as the monolayer spontaneous curvature, $K_{0,\mathrm{m}}$. Alternatively, one can consider the membrane as a 3D elastic medium[10–12] to incorporate the effects of internal stresses within the membrane and lipid structure such as tilt–curvature coupling.[13] The 3D elastic energy density of the membrane is obtained by a strain expansion in terms of the local stress and elasticity tensors. In general, these quantities vary spatially and must be integrated over the system volume to obtain the total elastic energy. Tilt–curvature theories[13–16] group together like terms in the 3D elastic energy density and integrate over the thickness of the membrane to obtain relations for the macroscopic elastic constants such as κ and $\bar{\kappa}$ as moments of the microscopic local stress and elasticity profiles. This process requires making many assumptions about the nature of lipid membranes, including lateral fluidity and incompressibility, which have not been directly validated due to the difficulty of locally measuring these quantities experimentally or computationally.

The local stress tensor, $\sigma_{ij}(\boldsymbol{x})$, of lipid bilayers and the corresponding lateral stress profile, $\sigma_{\mathrm{L}}(z) = (\sigma_{xx}(z) + \sigma_{yy}(z))/2 - \sigma_{zz}(z)$, are routinely obtained from molecular dynamics (MD) simulations[17–24] using the Irving–Kirkwood–Noll procedure.[25–29] However, computation of local elastic moduli of membranes has only recently gathered attention, despite its importance. Campelo *et al.*[30] computed the transmembrane lateral stretch modulus profile[13,31] of a coarse-grained (CG) MARTINI[32] bilayer by measuring the change in the lateral stress profile relative to the area strain:

$$\lambda_{\mathrm{L}}(z) = a_0 \frac{\partial \sigma_{\mathrm{L}}(z)}{\partial a}, \tag{1}$$

where a_0 is the area of the unstrained system. The monolayer $\lambda_{\mathrm{L}}(z)$ can be used to estimate the position of the neutral surface as well as the bending modulus.[13–16] Foley and Deserno[31,33] have recently computed $\lambda_{\mathrm{L}}(z)$ for the CG Cooke model and used it to estimate the position of the neutral surface. As pointed out by Kalutskii *et al.*,[34] one must be careful in the use of Eq. (1) as the variable elastic moduli along the membrane normal result in a nonuniform deformation of the membrane that requires a proper scaling of the z-coordinate when computing the change in local stress. Changes in the lateral stress profile with respect to variations in the ambient pressure have also been used to estimate the local Poisson ratio for MARTINI membranes.[34]

An alternate method to compute local elastic properties of lipid membranes is through the stress–stress fluctuation (SSF) method.[35–38] In the SSF method, materials are typically simulated in the canonical (NVT) or isothermal–isobaric[38] (NPT) ensembles, and the coefficients of the elasticity tensor, c_{ijkl}, are obtained from the sum of three contributions: a kinetic term that depends on the momenta of the particles, the fluctuations in the stress tensor, and the so-called Born term, which depends on the first and second derivatives of the potential.[35,36,39–43] Calculation of the Born term requires that multibody potentials that define angles or dihedrals be decomposed into central pairwise terms that depend only on the distances between particles.[21,22,29,43–46] The SSF method has been largely applied to characterize the elastic properties of solid (crystalline) and glassy systems.[35,36,44,45,47–50] Recently, Lips and Maass[38] computed the coefficients of the local elasticity tensor for a lipid membrane based on a single-tail CG lipid model[51,52] using Monte Carlo simulations. A key advantage of the SSF method is the ability to obtain all elastic coefficients from a single equilibrium simulation. In our companion paper,[53] we demonstrate the applicability of the SSF method to capture the elastic properties of solid and soft materials, such as molecular liquids, and provide methodological details on the numerical implementation in our custom code GROMACS-LS.[54]

The end goal of this paper is to characterize the local elastic properties of CG MARTINI interfacial systems, such as a water–hydrocarbon interface and a lipid membrane, via the SSF method. All local elastic coefficients are also validated through the explicit deformation method, in which changes in the local stress are measured relative to specific strains. In the first part, the liquid–liquid interface serves as a simple model to understand some of the unique features that transversely isotropic fluid systems possess. We show that the presence of the interface has important consequences for the elastic properties of the two immiscible liquids, such as softening compared to their pure states. We also show that some expected symmetries are locally broken due to the fluid nature of the system in combination with the constraint of mechanical equilibrium. In the remaining sections, we characterize the local elastic coefficients of a lipid membrane and explore their connection to tilt–curvature theories. We use the compliance tensor to formally define the local area, Young's, and bulk moduli, as well as the Poisson ratio from the elastic coefficients. We also compute various integrals of the area modulus to estimate the position of the neutral surface, as well as macroscopic moduli of area expansion and bending. Our results show that the SSF method is a powerful tool for characterizing the local elastic properties of biomaterials, such as lipid membranes, and for directly probing physical assumptions, such as lateral fluidity and incompressibility.

II. THEORY

A. Spatially resolved stress and elasticity tensors

In our companion paper,[53] we derive formulas to compute the whole-system Cauchy stress and elasticity tensors from MD simulations in the NVT ensemble (constant number of particles, volume, and temperature) using the method of dilatation. We refer the reader to the Theory section of that paper for a complete description of how these continuum quantities are macroscopically defined for molecular systems. Here, we focus on deriving the spatially resolved, or local, microscopic tensors. We begin by defining the Hamiltonian function for a system of N particles in the canonical ensemble as

$$H(\boldsymbol{r},\boldsymbol{p}) = \sum_{\alpha}^{N} \frac{|\boldsymbol{p}^{\alpha}|^2}{2m^{\alpha}} + U(\boldsymbol{r}^{\alpha}), \tag{2}$$

where $\boldsymbol{r} = \left(\boldsymbol{r}^1, \ldots, \boldsymbol{r}^{\alpha}, \ldots, \boldsymbol{r}^N\right)$ and $\boldsymbol{p} = \left(\boldsymbol{p}^1, \ldots, \boldsymbol{p}^{\alpha}, \ldots, \boldsymbol{p}^N\right)$ are the positions and momenta, m^{α} is the mass of particle α, and U is the internal energy. The partition function of such a system is defined as

$$Z = \frac{1}{h^{3N} N_A! N_B! \ldots} \int \exp\left(-\beta H(\boldsymbol{r},\boldsymbol{p})\right) d\boldsymbol{r}d\boldsymbol{p}, \tag{3}$$

where $\beta = \frac{1}{k_{\mathrm{B}}T}$, h is Planck's constant, N_X is the number of particles of species X, and $N = \sum_X N_X$. From this, one can define the canonical, or Helmholtz, free energy as

$$A = -\frac{1}{\beta} \ln(Z). \tag{4}$$

Similarly, the expectation value of an observable $Q(\boldsymbol{r},\boldsymbol{p})$ can be obtained from

$$\langle Q \rangle = \frac{1}{Z h^{3N} N_A! N_B! \ldots} \int Q(\boldsymbol{r},\boldsymbol{p}) \exp\left(-\beta H(\boldsymbol{r},\boldsymbol{p})\right) d\boldsymbol{r}d\boldsymbol{p}. \tag{5}$$

The local Cauchy stress is typically defined using the Irving–Kirkwood–Knoll procedure,[25–27] where mass, momentum, and energy pointwise fields are first defined and used within various balance equations to obtain a stress field that is valid for nonequilibrium systems. Alternatively, the local stress may

be derived geometrically from the Doyle–Ericksen formula[55–57] through the functional derivative,

$$\sigma_{ij}(\boldsymbol{x}) = 2\frac{\delta A}{\delta g_{ij}(\boldsymbol{x})}, \tag{6}$$

of the canonical free energy with respect to the ambient metric tensor field, $g_{ij}(\boldsymbol{x})$, which may vary inhomogeneously.[22,46,58,59] For ease of manipulation, we split the pointwise Cauchy stress into an ensemble average of the instantaneous kinetic and potential components:

$$\sigma_{ij}(\boldsymbol{x}) = \left\langle \sigma_{ij}^{\text{inst}}(\boldsymbol{x}) \right\rangle = \left\langle \sigma_{ij}^{\text{K,inst}}(\boldsymbol{x}) + \sigma_{ij}^{\text{U,inst}}(\boldsymbol{x}) \right\rangle. \tag{7}$$

The instantaneous kinetic component is defined as

$$\sigma_{ij}^{\text{K,inst}}(\boldsymbol{x}) = -\sum_{\alpha=1}^{N} \frac{1}{m^\alpha} g^{ik} g^{jl} p_k^\alpha p_l^\alpha \, \delta\left(\boldsymbol{r}^\alpha - \boldsymbol{x}\right), \tag{8}$$

where the lower and upper indices of the metric tensor refer to covariant and contravariant components, respectively, and g^{ij} denotes the components of the inverse of the metric tensor, satisfying $g^{ij}g_{jk} = \delta_k^i$. Assuming Cartesian coordinates, the instantaneous kinetic stress simplifies to

$$\sigma_{ij}^{\text{K,inst}}(\boldsymbol{x}) = -\sum_{\alpha=1}^{N} \frac{1}{m^\alpha} p_i^\alpha p_j^\alpha \, \delta\left(\boldsymbol{r}^\alpha - \boldsymbol{x}\right). \tag{9}$$

The instantaneous potential component is defined as

$$\sigma_{ij}^{\text{U,inst}}(\boldsymbol{x}) = \sum_{\substack{\alpha,\beta \\ \beta>\alpha}}^{N} \frac{\partial \mathring{U}}{\partial r^{\alpha\beta}} \frac{r_i^{\alpha\beta} r_j^{\alpha\beta}}{r^{\alpha\beta}} \, b\left(\boldsymbol{r}^\alpha, \boldsymbol{r}^\beta; \boldsymbol{x}\right), \tag{10}$$

where $b\left(\boldsymbol{r}^\alpha, \boldsymbol{r}^\beta; \boldsymbol{x}\right) = \int_0^1 \delta\left((1-s)\boldsymbol{r}^\alpha + s\boldsymbol{r}^\beta - \boldsymbol{x}\right) ds$ is the so-called bond function and we have replaced the potential $U(\boldsymbol{r}^\alpha)$ with a sum of central pairwise potential terms $\mathring{U}(r^{\alpha\beta})$, such that

$$U(\boldsymbol{r}^\alpha) = \sum_{\beta \neq \alpha} \mathring{U}(r^{\alpha\beta}). \tag{11}$$

Here, $r^{\alpha\beta} = |\boldsymbol{r}^{\alpha\beta}|$ is the distance between two interacting particles, α and β, and $\boldsymbol{r}^{\alpha\beta} = \boldsymbol{r}^\beta - \boldsymbol{r}^\alpha$. Assuming that interatomic potentials are conservative scalar functions of the particle positions,[29,43] which is true for most classical potentials used in MD simulations, we can replace the first derivatives of the potential, that is, the net forces acting on the particles, with a sum of central pairs:

$$\frac{\partial U}{\partial r_i^\alpha} = -\sum_{\beta \neq \alpha} \frac{\partial \mathring{U}}{\partial r^{\alpha\beta}} \frac{r_i^{\alpha\beta}}{r^{\alpha\beta}}. \tag{12}$$

An N-body potential can in general be decomposed into $\frac{1}{2}N(N-1)$ possible pairs.[22,29,43,46]

Extending the analogy to the Doyle–Ericksen derivation,[55–57] we geometrically define the local spatial elasticity tensor by taking the derivative of $\sigma_{ij}(\boldsymbol{x})$ with respect to the ambient metric:

$$c_{ijkl}(\boldsymbol{x}) = 2\frac{\partial \left\langle \sigma_{ij}^{\text{inst}}(\boldsymbol{x}) \right\rangle}{\partial g_{kl}}, \tag{13}$$

where in this case the metric is assumed to vary homogeneously everywhere in the system. One could in principle define a more general two-point elasticity tensor by taking another functional derivative of the local stress with respect to the metric field. However, analysis and physical interpretation of such a two-point tensor would pose a significant challenge as it describes the change in stress at $\boldsymbol{x}$ due to a local deformation at $\boldsymbol{y}$, which is beyond the scope of the current paper. Returning to Eq. (13), the derivative of the ensemble average of the local stress can be expanded as

$$c_{ijkl}(\boldsymbol{x}) = \frac{2}{h^{3N} N_A! N_B! \ldots} \frac{\partial}{\partial g_{kl}} \left(\frac{1}{Z} \int \sigma_{ij}^{\text{inst}}(\boldsymbol{x}) \exp\left(-\beta H\right) \, d\boldsymbol{r}d\boldsymbol{p} \right), \tag{14}$$

$$\begin{aligned} &= \frac{2}{Z h^{3N} N_A! N_B! \ldots} \int \frac{\partial \sigma_{ij}^{\text{inst}}(\boldsymbol{x})}{\partial g_{kl}} \exp\left(-\beta H\right) \, d\boldsymbol{r}d\boldsymbol{p} \\ &\quad - \frac{2\beta}{Z h^{3N} N_A! N_B! \ldots} \int \sigma_{ij}^{\text{inst}}(\boldsymbol{x}) \frac{\partial H}{\partial g_{kl}} \exp\left(-\beta H\right) \, d\boldsymbol{r}d\boldsymbol{p} \\ &\quad + \frac{2\beta}{\left(Z h^{3N} N_A! N_B! \ldots\right)^2} \left[\int \sigma_{ij}^{\text{inst}}(\boldsymbol{x}) \exp\left(-\beta H\right) \, d\boldsymbol{r}d\boldsymbol{p} \right. \\ &\quad \left. \times \int \frac{\partial H}{\partial g_{kl}} \exp\left(-\beta H\right) \, d\boldsymbol{r}d\boldsymbol{p} \right] \\ &= 2\left\langle \frac{\partial \sigma_{ij}^{\text{inst}}(\boldsymbol{x})}{\partial g_{kl}} \right\rangle - \beta V \left[\left\langle \sigma_{ij}^{\text{inst}}(\boldsymbol{x}) \bar{\sigma}_{kl}^{\text{inst}} \right\rangle - \left\langle \sigma_{ij}^{\text{inst}}(\boldsymbol{x}) \right\rangle \left\langle \bar{\sigma}_{kl}^{\text{inst}} \right\rangle \right], \end{aligned} \tag{15}$$

where $\bar{\sigma}_{kl}^{\text{inst}} = \frac{1}{V} \int \sigma_{kl}^{\text{inst}}(\boldsymbol{x}) \, d\boldsymbol{x}$ is the total instantaneous stress, that is, for the whole system, and we have used the relation $V\sigma_{kl}^{\text{inst}} = 2\frac{\partial H}{\partial g_{kl}}$.[46] Note that the second term of Eq. (15) is defined by the covariance of the instantaneous local stress with respect to the instantaneous total stress as the spatial dependence only appears explicitly in $\sigma_{ij}^{\text{inst}}(\boldsymbol{x})$. We split the first term inside the angle brackets in Eq. (15) into kinetic and potential terms for simplicity:

$$\frac{\partial \sigma_{ij}^{\text{inst}}(\boldsymbol{x})}{\partial g_{kl}} = \frac{\partial \sigma_{ij}^{\text{K,inst}}(\boldsymbol{x})}{\partial g_{kl}} + \frac{\partial \sigma_{ij}^{\text{U,inst}}(\boldsymbol{x})}{\partial g_{kl}}. \tag{16}$$

The kinetic term simplifies to

$$\begin{aligned} \frac{\partial \sigma_{ij}^{\text{K,inst}}(\boldsymbol{x})}{\partial g_{kl}} &= -\sum_{\alpha} \frac{1}{2m^\alpha} p_m^\alpha p_n^\alpha \left[g^{ik} g^{ml} g^{jn} + g^{mk} g^{il} g^{jn} + g^{im} g^{jk} g^{nl} \right. \\ &\quad \left. + g^{im} g^{nk} g^{jl} \right] \delta(\boldsymbol{r}^\alpha - \boldsymbol{x}), \end{aligned} \tag{17}$$

where we have used the identity $\frac{\partial g^{ij}}{\partial g_{kl}} = -\frac{1}{2}\left[g^{ik}g^{jl} + g^{il}g^{jk}\right]$ since $g^{ij}g_{jn} = \delta_n^i$. Particularizing now for Cartesian coordinates, we obtain

$$\begin{aligned} \frac{\partial \sigma_{ij}^{\text{K,inst}}(\boldsymbol{x})}{\partial g_{kl}} &= -\sum_{\alpha} \frac{1}{2m^\alpha} \left(p_l^\alpha p_j^\alpha \delta_{ik} + p_k^\alpha p_j^\alpha \delta_{il} + p_i^\alpha p_l^\alpha \delta_{jk} + p_i^\alpha p_k^\alpha \delta_{jl} \right) \\ &\quad \times \delta(\boldsymbol{r}^\alpha - \boldsymbol{x}). \end{aligned} \tag{18}$$

The potential component depends on both the first and second derivatives of the potential with respect to the pairwise distances:

$$\frac{\partial \sigma_{ij}^{\mathrm{U,inst}}(\boldsymbol{x})}{\partial g_{kl}} = \frac{1}{2}\sum_{\substack{\alpha,\beta \\ \beta>\alpha}}\left(\sum_{\substack{\gamma,\xi \\ \xi>\gamma}} \frac{\partial^2 \mathring{U}}{\partial r^{\gamma\xi}\partial r^{\alpha\beta}} \frac{r_i^{\alpha\beta} r_j^{\alpha\beta} r_k^{\gamma\xi} r_l^{\gamma\xi}}{r^{\alpha\beta} r^{\gamma\xi}} - \frac{\partial \mathring{U}}{\partial r^{\alpha\beta}} \frac{r_i^{\alpha\beta} r_j^{\alpha\beta} r_k^{\alpha\beta} r_l^{\alpha\beta}}{(r^{\alpha\beta})^3}\right) \times b(\boldsymbol{r}^\alpha, \boldsymbol{r}^\beta; \boldsymbol{x}), \tag{19}$$

where in the second derivative we must consider a second potentially independent pair of particles, γ and ξ, although the bond function only distributes the potential contribution along the path that connects particles α and β. These two particle pairs would be the same in the case of a two-body potential, but may be different in the case of three-body or higher order multibody potentials.

Putting it all together, we obtain the local version of the SSF formula for the elasticity tensor, as previously obtained by Lutsko:[35,38]

$$c_{ijkl}(\boldsymbol{x}) = c_{ijkl}^{0}(\boldsymbol{x}) + c_{ijkl}^{\mathrm{F}}(\boldsymbol{x}) + c_{ijkl}^{\mathrm{K}}(\boldsymbol{x}), \tag{20a}$$

$$c_{ijkl}^{0}(\boldsymbol{x}) = \left\langle \sum_{\substack{\alpha,\beta \\ \beta>\alpha}}\left(\sum_{\substack{\gamma,\xi \\ \xi>\gamma}} \frac{\partial^2 \mathring{U}}{\partial r^{\gamma\xi}\partial r^{\alpha\beta}} \frac{r_i^{\alpha\beta} r_j^{\alpha\beta} r_k^{\gamma\xi} r_l^{\gamma\xi}}{r^{\alpha\beta} r^{\gamma\xi}} - \frac{\partial \mathring{U}}{\partial r^{\alpha\beta}} \frac{r_i^{\alpha\beta} r_j^{\alpha\beta} r_k^{\alpha\beta} r_l^{\alpha\beta}}{(r^{\alpha\beta})^3}\right) b(\boldsymbol{r}^\alpha, \boldsymbol{r}^\beta; \boldsymbol{x})\right\rangle, \tag{20b}$$

$$c_{ijkl}^{\mathrm{F}}(\boldsymbol{x}) = -\beta V\left(\langle \sigma_{ij}^{\mathrm{inst}}(\boldsymbol{x})\tilde{\sigma}_{kl}^{\mathrm{inst}}\rangle - \langle \sigma_{ij}^{\mathrm{inst}}(\boldsymbol{x})\rangle\langle \tilde{\sigma}_{kl}^{\mathrm{inst}}\rangle\right), \tag{20c}$$

$$c_{ijkl}^{\mathrm{K}}(\boldsymbol{x}) = \left\langle \sum_{\alpha} \frac{1}{m^\alpha}\left(p_l^\alpha p_j^\alpha \delta_{ik} + p_k^\alpha p_j^\alpha \delta_{il} + p_i^\alpha p_l^\alpha \delta_{jk} + p_i^\alpha p_k^\alpha \delta_{jl}\right)\delta(\boldsymbol{r}^\alpha - \boldsymbol{x})\right\rangle. \tag{20d}$$

The Born term, c_{ijkl}^{0}, corresponds to the adiabatic elasticity at $T = 0$ K, and it represents the intrinsic elastic response of the material due to interatomic interactions. The fluctuation term, c_{ijkl}^{F}, corresponds to the covariance of the stress tensor, which is determined by the energy fluctuations within the material. Finally, the kinetic term, c_{ijkl}^{K}, is obtained from the momenta of the particles in the system. In general, the Born term tends to have positive values, while the fluctuation term tends to be negative. Inclusion of pair potentials such as Lennard-Jones potentials that are truncated at a given cutoff requires impulsive corrections to accurately compute the contributions to the stress and elasticity tensors from the first and second derivatives of the potential, depending on the shifting scheme (see our companion paper[53]).

To obtain continuum stress and elasticity fields, the pointwise quantities are convoluted with a weighting function $w(\boldsymbol{x}; \boldsymbol{y})$, supported in a domain $\Omega_{\boldsymbol{x}}$ that is centered at $\boldsymbol{x}$, which weights the contributions to the stress or elasticity for particles located at $\boldsymbol{y}$ in $\Omega_{\boldsymbol{x}}$ (see Methods). The weighting function must be normalized such that $\int_{\Omega_{\boldsymbol{x}}} w(\boldsymbol{x}; \boldsymbol{y})d\boldsymbol{y} = 1$. To apply the convolution to the potential contributions to the stress or elasticity, the weighting function must be integrated over the line segment that connects particles α and β, which is performed by the bond function $b(\boldsymbol{r}^\alpha, \boldsymbol{r}^\beta; \boldsymbol{x}) = \int_{s=0}^{1} w(\boldsymbol{x}; (1-s)\boldsymbol{r}^\alpha + s\boldsymbol{r}^\beta)$.

Classical molecular systems are often parametrized using bonded potentials such as harmonic bonds (2-body), harmonic or cosine angles (3-body), and harmonic or cosine dihedrals (4-body), among many others. Any 3-body or higher order potentials must be carefully included in the Born term [Eq. (20b)] as we need to cast the potentials in terms of pairwise distances.[43–45] For a harmonic angle potential acting on particles α, β, and γ, one can define the potential and its derivatives explicitly in terms of pairwise distances ($r^{\alpha\beta}$, $r^{\alpha\gamma}$, and $r^{\beta\gamma}$) using various identities including the dot product and the law of cosines. Once the first and second derivatives of the three-body angle potential have been obtained, one must then incorporate nine different contributions into the first term of Eq. (20b), which correspond to the three homo-pairs $\{r^{\alpha\beta}, r^{\alpha\beta}\}$, $\{r^{\alpha\gamma}, r^{\alpha\gamma}\}$, and $\{r^{\beta\gamma}, r^{\beta\gamma}\}$ as well as the six hetero-pairs $\{r^{\alpha\beta}, r^{\alpha\gamma}\}$, $\{r^{\alpha\gamma}, r^{\alpha\beta}\}$, $\{r^{\alpha\beta}, r^{\beta\gamma}\}$, $\{r^{\beta\gamma}, r^{\alpha\beta}\}$, $\{r^{\alpha\gamma}, r^{\beta\gamma}\}$, and $\{r^{\beta\gamma}, r^{\alpha\gamma}\}$. Note that swapping the order of the hetero-pairs produces different contributions to the Born term, even though the second derivatives of the potential are interchangeable due to Schwarz's theorem, for example,

$$\frac{\partial^2 \mathring{U}}{\partial r^{\beta\gamma}\partial r^{\alpha\beta}} = \frac{\partial^2 \mathring{U}}{\partial r^{\alpha\beta}\partial r^{\beta\gamma}}. \tag{21}$$

Definitions of all the bonded and nonbonded interatomic potentials used in this study, including their first and second derivatives, are provided in the supplementary material of our companion paper.[53]

In general, the elasticity tensor has $81 = 3^4$ individual elements, yet the number of unique terms in $c_{ijkl}(\boldsymbol{x})$ depends on the symmetries that are applicable. Symmetries in the stress and strain tensors under the constraint of linear elasticity result in minor symmetries of the form $c_{ijkl} = c_{jikl} = c_{ijlk}$. Symmetry of the strain energy density with respect to the strain components results in major symmetries of the form $c_{ijkl} = c_{klij}$. When integrated over the whole system, both minor [e.g., $\int c_{yzyz}(\boldsymbol{x})d\boldsymbol{x} = \int c_{zyzy}(\boldsymbol{x})d\boldsymbol{x}$] and major [e.g., $\int c_{yyzz}(\boldsymbol{x})d\boldsymbol{x} = \int c_{zzyy}(\boldsymbol{x})d\boldsymbol{x}$] symmetries must apply, and therefore the number of unique elements in the elasticity tensor reduces to 21. However, as we will show in the Results and Discussion section, major symmetries may sometimes be broken locally depending on the geometry and physical state of the system. Assuming only minor symmetries, we can write the 36 possibly unique elements of the local elasticity tensor as the 6×6 stiffness matrix:

$$c_{mn} = \begin{bmatrix} c_{11} & c_{12} & c_{13} & c_{14} & c_{15} & c_{16} \\ c_{21} & c_{22} & c_{23} & c_{24} & c_{25} & c_{26} \\ c_{31} & c_{32} & c_{33} & c_{34} & c_{35} & c_{36} \\ c_{41} & c_{42} & c_{43} & c_{44} & c_{45} & c_{46} \\ c_{51} & c_{52} & c_{53} & c_{54} & c_{55} & c_{56} \\ c_{61} & c_{62} & c_{63} & c_{64} & c_{65} & c_{66} \end{bmatrix}, \tag{22}$$

where we have omitted the spatial dependence on $\boldsymbol{x}$ for simplicity and use Voigt notation:

Tensor index:	xx	yy	zz	yz or zy	xz or zx	xy or yx
Voigt index:	1	2	3	4	5	6

Here, we focus on systems that are transversely isotropic in the x–y plane such as liquid–liquid interfaces or lipid bilayers. As such, any locally computed fields only vary along the z-direction. Furthermore, these systems are fluid in the plane of isotropy, which imposes the additional constraint that the lateral stress must be uniform [i.e.,

$\sigma_{xx}(z) = \sigma_{yy}(z)$]. The stiffness matrix for this type of system reduces to

$$c_{mn} = \begin{bmatrix} c_{11} & c_{12} & c_{13} & 0 & 0 & 0 \\ c_{12} & c_{11} & c_{13} & 0 & 0 & 0 \\ c_{31} & c_{31} & c_{33} & 0 & 0 & 0 \\ 0 & 0 & 0 & c_{44} & 0 & 0 \\ 0 & 0 & 0 & 0 & c_{44} & 0 \\ 0 & 0 & 0 & 0 & 0 & c_{66} \end{bmatrix}, \tag{23}$$

where the in-plane symmetry and lateral fluidity require that $c_{11}(z) = c_{22}(z), c_{12}(z) = c_{21}(z), c_{13}(z) = c_{23}(z), c_{31}(z) = c_{32}(z)$, and $c_{44}(z) = c_{55}(z)$, as the system is physically indistinguishable in the x–y plane. For transversely isotropic systems, the in-plane shear modulus $c_{66}(z)$ is also coupled to $c_{11}(z)$ and $c_{12}(z)$ through the relation $c_{66}(z) = \frac{1}{2}(c_{11}(z) - c_{12}(z))$.

B. Hooke's law, stress–strain coefficients, and explicit deformation

The values of the elasticity tensor obtained with the SSF formula [Eq. (20a)] correspond to the coefficients in an unstressed state where $\sigma_{ij} = 0$. However, the coefficients obtained from stress–strain relations, that is, Hooke's law, differ for systems where $\sigma_{ij} \neq 0$.[41,42,45,60–62] The incremental change in Cauchy stress around a pre-stressed configuration is not determined solely by the material modulus c_{ijkl}, but must also include additional terms that depend explicitly on the initial stress σ_{ij}.[61,62] This is because the stress rate must be taken in an objective sense using the Truesdell rate.[43] For an infinitesimal strain increment ϵ_{kl} relative to the pre-stressed configuration, the change in stress is given by

$$\Delta\sigma_{ij} = [c_{ijkl} + \sigma_{jl}\delta_{ik} + \sigma_{jk}\delta_{il} - \sigma_{ij}\delta_{kl}]\epsilon_{kl}, \tag{24}$$

where summations are carried out over repeated Roman indices. This relation can be cast into the standard form $\Delta\sigma_{ij} = \tilde{c}_{ijkl}\epsilon_{kl}$, where the effective tangent modulus $\tilde{c}_{ijkl}$ incorporates both the material stiffness and the geometric contributions due to the pre-stress. By symmetrizing the stress–strain contractions, we obtain a relation for the elasticity tensor under a finite Cauchy stress:

$$\tilde{c}_{ijkl}(\boldsymbol{x}) = c_{ijkl}(\boldsymbol{x}) + \frac{1}{2}\big[\sigma_{ik}(\boldsymbol{x})\delta_{jl} + \sigma_{il}(\boldsymbol{x})\delta_{jk} + \sigma_{jk}(\boldsymbol{x})\delta_{il} + \sigma_{jl}(\boldsymbol{x})\delta_{ik} - 2\sigma_{ij}(\boldsymbol{x})\delta_{kl}\big]. \tag{25}$$

Following Wallace,[61] we refer to the elements of $\tilde{c}_{ijkl}$ as stress–strain coefficients (also known as Birch coefficients[61,63]) as they are the effective values that would be obtained by explicitly deforming the material experimentally or computationally. The values of $\tilde{c}_{ijkl}$ only differ from c_{ijkl} for systems where the Cauchy stress is nonzero due to loading conditions or for nonuniform systems, such as lipid membranes, where there is a large internal pre-stress.

Hooke's law defines the following relations for the change in local stress for a transversely isotropic system:

$$\Delta\sigma_{xx}(z) = \tilde{c}_{11}(z)\epsilon_{xx} + \tilde{c}_{12}(z)\epsilon_{yy} + \tilde{c}_{13}(z)\epsilon_{zz}, \tag{26}$$

$$\Delta\sigma_{yy}(z) = \tilde{c}_{12}(z)\epsilon_{xx} + \tilde{c}_{11}(z)\epsilon_{yy} + \tilde{c}_{13}(z)\epsilon_{zz}, \tag{27}$$

$$\Delta\sigma_{zz}(z) = \tilde{c}_{31}(z)\epsilon_{xx} + \tilde{c}_{31}(z)\epsilon_{yy} + \tilde{c}_{33}(z)\epsilon_{zz}, \tag{28}$$

$$\Delta\sigma_{yz}(z) = 2\tilde{c}_{44}(z)\epsilon_{yz}, \tag{29}$$

$$\Delta\sigma_{xz}(z) = 2\tilde{c}_{44}(z)\epsilon_{xz}, \tag{30}$$

$$\Delta\sigma_{xy}(z) = 2\tilde{c}_{66}(z)\epsilon_{xy}, \tag{31}$$

where the stress–strain coefficients are written in Voigt notation for convenience. We use these relations with constrained deformations to obtain the individual elements of $\tilde{c}_{mn}$. Consider a deformation that keeps the system area fixed at the equilibrium value $a = a_0$, while the system is elongated or compressed along the z-direction. Under such conditions, the lateral strain is zero ($\epsilon_{xx} = \epsilon_{yy} = 0$) and $\epsilon_{zz} = \Delta z/z_0$; therefore, Eqs. (26) and (27) can be combined to obtain

$$\tilde{c}_{13}^{\mathrm{ED}}(z) = \frac{z_0}{2}\left.\frac{\partial(\sigma_{xx}(z) + \sigma_{yy}(z))}{\partial z}\right|_{a=a_0}. \tag{32}$$

Under the same deformation conditions, Eq. (28) can be simplified to obtain

$$\tilde{c}_{33}^{\mathrm{ED}}(z) = z_0\left.\frac{\partial\sigma_{zz}(z)}{\partial z}\right|_{a=a_0}. \tag{33}$$

Similarly, consider a deformation that keeps the system's z box dimension fixed at the equilibrium value $z = z_0$ while the area of the system is expanded or compressed. As such, there is no strain in the z-direction ($\epsilon_3 = 0$) and the lateral strain is given by $\epsilon_{xx} + \epsilon_{yy} \approx \frac{a-a_0}{a_0}$, which, when combined with Eqs. (26)–(28), results in the relations

$$\frac{(\tilde{c}_{11}(z) + \tilde{c}_{12}(z))^{\mathrm{ED}}}{2} = \frac{a_0}{2}\left.\frac{\partial(\sigma_{xx}(z) + \sigma_{yy}(z))}{\partial a}\right|_{z=z_0} \tag{34}$$

and

$$\tilde{c}_{31}^{\mathrm{ED}}(z) = a_0\left.\frac{\partial\sigma_{zz}(z)}{\partial a}\right|_{z=z_0}. \tag{35}$$

In the ED method, the coefficients $\tilde{c}_{11}(z)$ and $\tilde{c}_{12}(z)$ cannot be individually probed for a fluid transversely isotropic system, as any equilibrium lateral deformation, even if performed uniaxially, results in an equal lateral stress distribution, $\sigma_{xx}(z) = \sigma_{yy}(z)$. This can also be interpreted as these two stress–strain elastic coefficients being equal, $\tilde{c}_{11}(z) = \tilde{c}_{12}(z)$. The shear stress–strain coefficients $\tilde{c}_{44}(z)$ and $\tilde{c}_{66}(z)$ can be obtained directly from Eqs. (30) and (31) by applying volume-preserving simple shear deformations in the y–z plane ($\epsilon_{yz} = \frac{\Delta y}{z}$) or the x–y plane ($\epsilon_{xy} = \frac{\Delta x}{y}$), respectively.

III. METHODS

Molecular dynamics (MD) simulations were performed with the GROMACS simulation package v2020.[64] A custom version of the GROMACS-LS software,[21,22,46,54] which integrates GROMACS v2016 with the MDStress library, was used to run simulations to estimate the elastic coefficients using the SSF method [Eq. (20a)]. See our companion paper[53] for technical details of the SSF implementation, including treatment of truncated pair potentials, first

and second derivatives of multibody potentials, and convergence analysis. The MARTINI 3.0 force field[65] was used for all the coarse-grained (CG) liquid and membrane systems. The Lennard-Jones potential was truncated using a plain cutoff with a shift at r_{cut} = 1.1 nm as suggested by the MARTINI force field. Newton's equations of motion were integrated using the leapfrog algorithm with a time step of 0.005 ps. This shorter time step was chosen to obtain physically consistent elastic coefficients as described in our companion paper.[53] Temperature was held constant using the velocity-rescaling thermostat of Bussi *et al.*[66] with a coupling time constant of 1.0 ps. For constant-pressure simulations, the pressure was maintained semi-isotropically with the cell-rescaling barostat of Bernetti and Bussi.[67] with a coupling time constant of 5.0 ps. The pressure and temperature coupling were performed at every simulation step to avoid incorrect calculation of the instantaneous pressure in CG systems because of improper setting of parameters for generating neighbor lists, which has been recently reported by Kim *et al.*[68] Specifically for GROMACS, this translates to setting the following simulation input parameters: `nsttcouple = 1`, `nstpcouple = 1`, and `verlet-buffer-tolerance = 0.0005`. The local stress/elasticity implementation in GROMACS-LS uses trilinear weight functions to define $w(\boldsymbol{x};\, \boldsymbol{r}^{\alpha} - \boldsymbol{x})$ and $b(\boldsymbol{r}^{\alpha}, \boldsymbol{r}^{\beta};\, \boldsymbol{x})$ that are used to discretize the resulting fields as described in detail by Vanegas *et al.*[21] Impulsive corrections to the truncated Lennard-Jones potential contributions were computed using a width of 1×10^{-5} nm (see our companion paper[53]).

A water–dodecane interfacial system was built by first generating two slabs of the pure liquids with the *insane* program[69] of roughly the same dimensions ($6 \times 6 \times 5$ nm^3) and stacking them together in the z-direction so that the system is isotropic in the x–y plane. The combined system contains 512 CG dodecane and 1379 CG water molecules. This initial configuration was first energy minimized and then equilibrated under constant area, temperature, and normal pressure (NP_zaT) for a total time of 200 ns. This was followed by a production run under the same conditions for a total time of 1000 ns storing the particle positions and velocities every 5 ps. From this NP_zaT production run, a simulation frame was extracted that most closely matched the average box dimensions and volume. This box-average frame was then used to set up five independent simulation replicas with different initial velocities to compute the local elasticity and stress tensors. Each replica was simulated at constant volume (NVT) for a total time of 3000 ns. The local elastic coefficients $c_{nm}(z)$ and stress $\sigma_i(z)$ were obtained from the average of the five replicas using a grid spacing of 0.1 nm in the z-direction and sampling every 50 steps.

Two 1,2-dioleoyl-sn-glycero-3-phosphocholine (DOPC) bilayers containing either 200 CG lipids and 2980 CG water molecules or 128 CG lipids and 1920 water molecules were constructed with the *insane* program. These DOPC systems were first energy minimized and then equilibrated under temperature and pressure (NPT) for a total time of 200 ns. This was followed by a production run under the same conditions for a total time of 1000 ns storing the particle positions and velocities every 5 ps. From this NPT production run, a simulation frame was extracted that most closely matched the average box dimensions. This box-average frame was then used to set up five independent simulation replicas with different initial velocities to compute the local elasticity and stress tensors. Each replica was simulated at constant volume (NVT) for a total time of 5000 ns. The local elastic coefficients $c_{mn}(z)$ and stress $\sigma_{ij}(z)$ were obtained from the average of the five replicas using a grid spacing of 0.1 nm in the z-direction and sampling every 50 steps. An additional large DOPC system, containing 1800 lipids and 26 800 waters, was simulated using the same equilibration (200 ns) and constant temperature and pressure protocol (1000 ns) to estimate elastic properties (e.g., the bending modulus) of the membrane with independent methods. This large DOPC trajectory, saved at 100 ps intervals, was analyzed using three different methods: (1) power spectra fluctuations[14,15,70] using the PO4 beads to define the surface; (2) lipid director fluctuations[71–73] using the PO4 and C4* beads to define the director field and Z-normalization; and (3) spatial extent (SPEX).[74] The power spectrum and lipid director fluctuations were analyzed with Python code from the group of Markus Deserno, available from https://github.com/mferguder/Membrane-Fluctuation-Documentation. The spatial extent analysis was carried out with the MembraneAnalysis.jl code, available from https://github.com/amiralih/MembraneAnalysis.jl.

The local stress–strain coefficients $\tilde{c}_{nm}(z)$ were also computed from explicit deformation simulations by computing the change in the local stress relative to a given strain [Eqs. (29)–(35)]. The z-coordinates of all deformed systems were uniformly scaled to match the dimensions of the undeformed configuration before performing the linear fits to determine the local coefficients. In practice, the uniform scaling is accomplished by using the same grid size for all systems, regardless of the z-box dimension. Systems were simulated under three constrained ensembles: (1) NP_zaT, where the area in the x–y plane was fixed at the average value and the pressure in the z-direction was kept constant at 1 atm for 1000 ns; (2) $NP_{xy}ZT$, where the z box dimension was fixed at the average value, and the pressure in the x–y plane was kept constant semi-isotropically for 1000 ns at the average value obtained for each system: −65.5 atm for water–dodecane and 1 atm for DOPC; and (3) NVT with the equilibrium simulation box sheared in the y–z or x–y planes for 100 ns each. For the first two constant pressure ensembles, a set of 19 frames was extracted that spans the range of the 10th to 90th percentile (p) of the simulation volumes computed over the length of the trajectory. One frame was extracted that matched the average volume ($p = 0.50$), while nine frames were uniformly extracted in each of the compressive ($0.10 \le p < 0.50$) and expansive ($0.50 < p \le 0.90$) regimes. Each of these ED simulations was run under constant volume and temperature (NVT) for a total time of 500 ns for DOPC and 1000 ns for water–dodecane. The coefficients for the compressive and expansive regimes were independently computed using an equal grid size and then averaged to obtain the final values of the stress–strain coefficients. For the shear simulations, ten frames were extracted from each of the nonequilibrium box-deformation trajectories and equilibrated for 100 ns. Each of these 20 shear ED simulations was then run under constant volume and temperature (NVT) for a total time of 500 ns for DOPC and 1000 ns for water–dodecane. The local stress for systems in which the box is not rectangular must first be transformed by a rotation matrix, where the angle is given by the relation $\tan\phi = \epsilon_{ij}$, before computing the stress–strain shear coefficients using Eqs. (29) and (31). The lateral stretch modulus profile, $\lambda_L(z)$, of the DOPC membrane was estimated using Eq. (1) by simulating 19 systems with

frames extracted from the equilibrium *NPT* trajectory that span the range of the 10th to 90th percentile of the simulated areas. Each frame was then equilibrated under constant area and ambient normal pressure (NP_zaT) for 100 ns and subsequently simulated for 1000 ns to compute the lateral stress profile at each fixed area. All data analysis and plots were created using the Python NumPy, SciPy, and Matplotlib libraries.[75–77]

IV. RESULTS AND DISCUSSION

A. Local elasticity profiles across a liquid-liquid interface

We first analyze a simple liquid–liquid interface composed of layers of MARTINI CG water and dodecane and compute the local elastic coefficients using the SSF method, as shown in Fig. 1. This interfacial system is transversely isotropic in the x–y plane, and therefore the elastic coefficients only vary along the z direction. The z-profiles for the coefficients $c_{11}(z)$ and $c_{22}(z)$ are equal to each other as expected from the symmetry of the system, and their values decrease in the vicinity of the interface ($z \approx \pm 2$ nm) because of the lower material density in this region [Fig. 1(a)]. Surprisingly, these local coefficients are significantly smaller in magnitude than the observed c_{11} values for either of the pure liquids [dotted red and gray lines in Fig. 1(a)]. A similar pattern is observed for the off-diagonal coefficients $c_{12}(z)$ and $c_{21}(z)$ [Fig. 1(a)], where the values decrease near the interface and the magnitudes are smaller than the bulk values. The average of the stress–strain coefficients $\tilde{c}_{11}(z)$ and $\tilde{c}_{12}(z)$ obtained with the explicit deformation method [Eq. (34)] is in excellent agreement with the values from the SSF formula as shown in Fig. 1(c). Because of the fluid nature of the liquid–liquid interface, the two coefficients $\tilde{c}_{11}(z)$ and $\tilde{c}_{12}(z)$ cannot be independently obtained with the explicit deformation method, as any strain will always result in a uniform change in the in-plane stresses σ_{xx} and σ_{yy}.

To further explore the large decrease in the values of the local elasticity profiles compared to the values obtained for the pure liquids, we take a closer look at the individual contributions from the Born, fluctuation, and kinetic terms to $c_{11}(z)$. The z-profile of the Born term [Fig. 2(a)] clearly shows that $c_{11}^0(z)$ is significantly smaller at the interface because of the lower density, but reaches the expected values of the pure liquids, either water or dodecane,

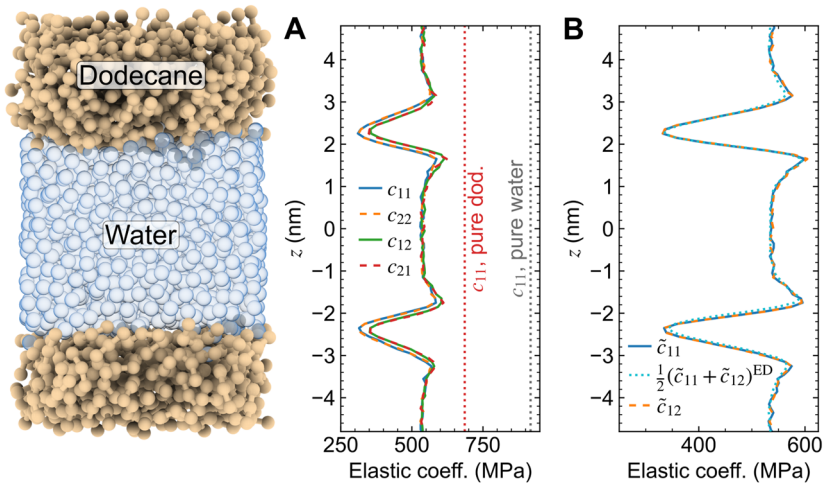

FIG. 1. Local elasticity profiles of a MARTINI water–dodecane interface. (a) Coefficients that couple stress and strain in the x–y plane: c_{11}, c_{12}, c_{21}, and c_{22}. (b) Stress–strain coefficients $\tilde{c}_{11}$ and $\tilde{c}_{12}$ compared to the average obtained with the explicit deformation (ED) method. Dotted lines in panel (a) show values obtained for the pure liquids (data from our companion paper[53]).

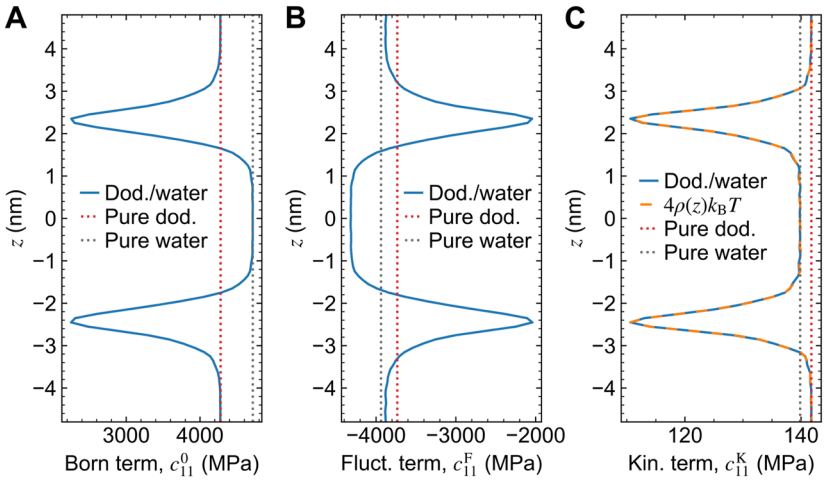

FIG. 2. Contributions from the Born [c_{11}^0, (a)], fluctuation [c_{11}^F, (b)], and kinetic [c_{11}^K, (c)] terms to the c_{11} coefficient for the dodecane–water interface. Panel (c) includes a comparison to $4\rho(z)k_BT$, where $\rho(z)$ is the number density. This relation for c_{11}^K is obtained by integrating the momentum terms in Eq. (20d) using the equipartition theorem. Dotted lines show values obtained for the pure liquids (data from our companion paper[53]).

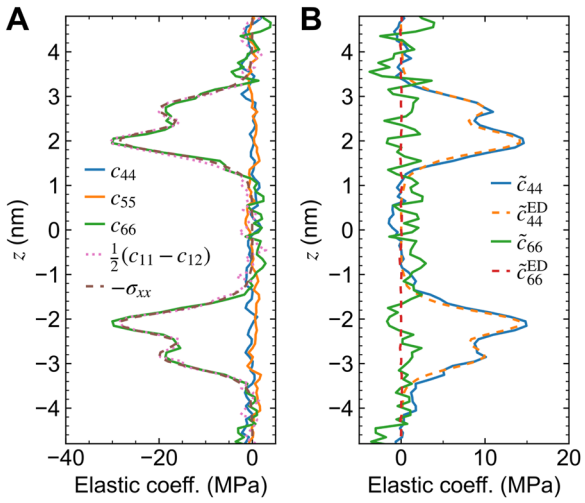

FIG. 3. Shear deformation elasticity profiles of a MARTINI water–dodecane interface. (a) Shear deformation coefficients c_{44} (y–z plane), c_{55} (x–z plane), and c_{66} (x–y plane). The negative of the lateral stress, $-\sigma_{xx}(z)$, shown for comparison. (b) Stress–strain coefficients $\tilde{c}_{44}$ and $\tilde{c}_{66}$ compared to the explicit deformation (ED) method.

at "bulk" z locations far enough from the interface. In contrast, the z-profile of $c_{11}^{F}(z)$ [Fig. 2(b)] shows that the stress fluctuations are larger in magnitude in the bulk liquid regions, as the values are more negative compared to pure water or dodecane (dotted red and gray lines). The kinetic term $c_{11}^{K}(z)$ [Fig. 2(c)] shows a similar pattern to the Born term, where the bulk values approach those observed in the pure liquids. Furthermore, $c_{11}^{K}(z)$ is proportional to the number density, $\rho(z)$, and matches exactly the relation $4\rho(z)k_BT$ [Fig. 2(c)], which is obtained by integrating the momentum terms in Eq. (20d) using the equipartition theorem.[38] It is clear from the Born and kinetic components that the individual liquids behave as expected in the bulk-like regions. However, the nature of the periodic boundary conditions, with infinitely alternating water and dodecane layers, leads to larger stress fluctuations than those normally observed for pure water or dodecane. This results in the unexpected softening of both liquids and demonstrates the importance of the fluctuation term in determining the mechanical properties of inhomogeneous materials at finite temperatures. As such, the elastic moduli of complex materials are not only determined by the inter- and intramolecular interactions but also by the stress fluctuations within the material. These fluctuations are likely dependent on many factors, such as simulation size, molecular features, and system geometry, which although interesting, are beyond the scope of the current study.

While the coefficients $c_{11}(z)$ and $c_{12}(z)$ appear very similar to each other, they need not be identical as long as they follow the transversely isotropic stability condition $\frac{1}{2}[c_{11}(z) - c_{12}(z)] = c_{66}(z)$. Indeed, the lateral shear coefficient $c_{66}(z)$, acting in the x–y plane, closely matches the stability condition as well as $-\sigma_{xx}(z)$ as shown in Fig. 3(a). We are not aware of any mathematical relation that would require the $c_{66}(z) = -\sigma_{xx}(z)$ for such a system. In contrast to the lateral shear, the transverse shear coefficients $c_{44}(z)$ (y–z plane) and $c_{55}(z)$ (x–z plane) fluctuate near zero [Fig. 3(a)]. The shear stress–strain elastic coefficients are in excellent agreement with the profiles obtained with the explicit deformation method, as shown in Fig. 3(b). Although noisy, it is clear that the stress–strain lateral shear coefficient $\tilde{c}_{66}(z)$ vanishes, which is consistent with the relation $\tilde{c}_{66} = c_{66} + \frac{1}{2}(\sigma_{xx} + \sigma_{yy})$ [obtained from Eq. (25)] and the empirical observation that $c_{66}(z) = -\sigma_{xx}(z) = -\sigma_{yy}(z)$. Similarly, the stress–strain transverse shear coefficient $\tilde{c}_{44}(z) = c_{44} + \frac{1}{2}(\sigma_{xx} + \sigma_{zz})$ takes a nonzero value because of the contribution from the local stress. The observation that the stress–strain transverse shear modulus, $\tilde{c}_{44}^{ED}(z)$, obtained by deforming the system, is nonzero is counterintuitive given the expectation that the off-diagonal elements of the stress should vanish, $\sigma_{yz}(z) = \sigma_{xz}(z) = 0$, for any fluid system at equilibrium. However, one needs to consider that the stress tensor in the nonrectangular sheared configuration is given by $\boldsymbol{\sigma}'(z) = \mathbf{R}^T\boldsymbol{\sigma}(z)\mathbf{R}$, where $\mathbf{R}$ is a rotation matrix about the axis not involved in the shear and the angle of rotation is given by $\tan\varphi = \epsilon_{ij}$. In the case of a simple xy shear deformation, the transformed stress is

$$\sigma'_{xy}(z) = [\sigma_{yy}(z) - \sigma_{xx}(z)]\sin\varphi\cos\varphi + \sigma_{xy}(z)\cos(2\varphi), \quad (36)$$

which vanishes as $\sigma_{xx}(z) = \sigma_{yy}(z)$ because of the transverse isotropy and $\sigma_{xy}(z) = 0$. However, in the case of a simple xz shear deformation, the transformed stress is

$$\sigma'_{xz}(z) = [\sigma_{xx}(z) - \sigma_{zz}(z)]\sin\varphi\cos\varphi + \sigma_{xz}(z)\cos(2\varphi), \quad (37)$$

which does not vanish even though $\sigma_{xz}(z) = 0$.

B. Broken major symmetry of local elastic coefficients

The z-profiles for elastic coefficients that couple σ_{zz} and/or ϵ_{zz} for the water–dodecane interface are shown in Fig. 4. The coefficients $c_{13}(z)$ and $c_{23}(z)$ are equal to each other as expected from the symmetry in the x–y plane, and their z-dependence is similar to that of $c_{12}(z)$. However, the coefficients $c_{31}(z)$ and $c_{32}(z)$, although equal to each other, are approximately constant across the interface [see Fig. 4(a)] and locally break the major symmetry of the elasticity tensor [i.e., $c_{13}(z) \neq c_{31}(z)$ and $c_{23}(z) \neq c_{32}(z)$]. Note that at the level of the whole system, the major symmetry is maintained, as the z-averaged values are numerically indistinguishable, $\bar{c}_{13} = \bar{c}_{31} = 537.43$ MPa. Furthermore, the coefficient $c_{33}(z)$ is also approximately constant across the interface [Fig. 4(a)] although its value is slightly larger ($\bar{c}_{33} = 553.8 \pm 2.3$ MPa), which matches the average values of $c_{11}(z)$ and $c_{22}(z)$ in the bulk-like dodecane and water regions.

To understand why the three local coefficients $c_{31}(z)$, $c_{32}(z)$, and $c_{33}(z)$ are constant across the liquid–liquid interface, we consider the equilibrium condition, which dictates that div $\boldsymbol{\sigma}(\boldsymbol{x}) = 0$ (i.e., no net forces act on the system). For a transversely isotropic system, the equilibrium condition simplifies to

$$\frac{\partial\sigma_{zz}(z)}{\partial z} = \frac{\partial}{\partial z}[c_{31}(z)\epsilon_{xx} + c_{32}(z)\epsilon_{yy} + c_{33}(z)\epsilon_{zz}] = 0. \quad (38)$$

This relation has two important consequences for the liquid–liquid interface: (i) $\sigma_{zz}(z)$, the normal component of the stress, must be constant, and (ii) $c_{31}(z)$, $c_{32}(z)$, and $c_{33}(z)$ must also be constant for Eq. (38) to be true for any strain values. Conceptually, the equilibrium condition for this liquid–liquid interface specifies that any strain acting in the x–y plane or in the z direction must induce

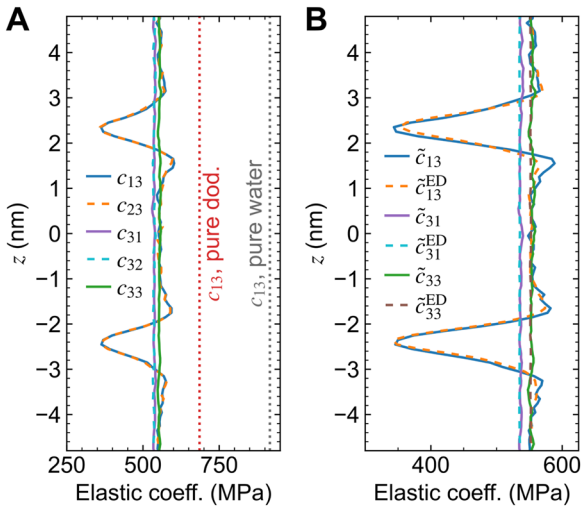

FIG. 4. Local elasticity profiles of a MARTINI water–dodecane interface. (a) Coefficients that couple σ_{zz} and/or ϵ_{zz}: c_{13}, c_{23}, c_{31}, c_{32}, and c_{33}. (b) Stress–strain coefficients $\tilde{c}_{13}$, $\tilde{c}_{31}$, and $\tilde{c}_{13}$ compared to the explicit deformation method (ED). Dotted lines in panel (a) show values obtained for the pure liquids (data from our companion paper[53]).

a uniform change in the normal stress, $\sigma_{zz}(z)$. Comparison of the SSF formula stress–strain coefficients $\tilde{c}_{13}(z)$, $\tilde{c}_{31}(z)$, and $\tilde{c}_{33}(z)$ with profiles obtained through the explicit deformation method [Eqs. (32) and (33)] in Fig. 4(b) shows excellent agreement and further validates the local breaking of the major symmetry of the elasticity tensor. A similar phenomenon is observed for the DOPC membrane system as will be shown in Sec. IV C.

C. Elasticity profiles of a DOPC lipid bilayer

Having established the expected behavior for the local elasticity profiles with the simple liquid–liquid interface, we now characterize the more complex and biologically relevant DOPC lipid membrane patch composed of 200 lipids (see Methods), which is also transversely isotropic in the x–y plane. The z-profiles for the coefficients that couple stress and strain in the x–y plane are shown in Fig. 5(a). Similarly to the water–dodecane interface, the in-plane symmetry and lateral fluidity in the DOPC bilayer result in $c_{11}(z) = c_{22}(z)$ and $c_{12}(z) = c_{21}(z)$. The values of $c_{11}(z)$ and $c_{12}(z)$ equal each other in the water region ($z > 3$ nm and $z < -3$ nm), as expected from the isotropy of the fluid, and generally follow the same trend of increased stiffness in the headgroup region followed by a softening at the hydrocarbon interface [Fig. 5(a)]. The stress–strain coefficients $\tilde{c}_{11}(z)$ and $\tilde{c}_{12}(z)$ are indistinguishable from each other as expected from the lateral fluidity and are also in excellent agreement with the average z-profile obtained from the explicit deformation method [Fig. 5(b)]. To test possible effects of system size, which may smear the z-profiles due to membrane undulations,[78,79] we also computed the local elastic coefficients for a smaller DOPC membrane with 128 lipids, while keeping the same water-to-lipid ratio, as shown in Fig. S1. No significant smearing is observed in the stress or elasticity profiles of the larger system compared to the smaller 128-lipid membrane; therefore, we continue the remaining analysis with the 200-lipid system.

In contrast to the simple water–dodecane system, where the coefficients had values much lower than those of the pure individual liquids, the $c_{11}(z)$ and $c_{12}(z)$ profiles for the DOPC membrane have values that are generally larger than those of pure water except near the hydrophobic–water interface [Fig. 5(a)]. To better understand this observation, we again turn to the individual contributions from the Born, fluctuation, and kinetic terms of c_{11} as shown in Fig. 6. The Born term [Fig. 6(a)] shows that values in the water region match those of the pure liquid and vary within the bilayer, roughly following the system density (larger near the phosphate headgroups and smaller near the bilayer midplane). The fluctuation term shown in Fig. 6(b) follows an opposing pattern compared to the Born term, with the water region showing less negative values compared to those of the pure liquid. This is in contrast to the water–dodecane interface, where the values of $c_{11}^{F}(z)$ were more negative compared to those of the pure liquids, which resulted in significant softening of the two liquids together. As the lipids are only able to freely diffuse laterally, energy exchange between the bilayer and the solvent is limited; therefore, the energy and stress fluctuations are also reduced. The kinetic contribution follows exactly the relation $4\rho(z)k_BT$ and the values in the water region closely match those of the pure liquid [Fig. 6(c)].

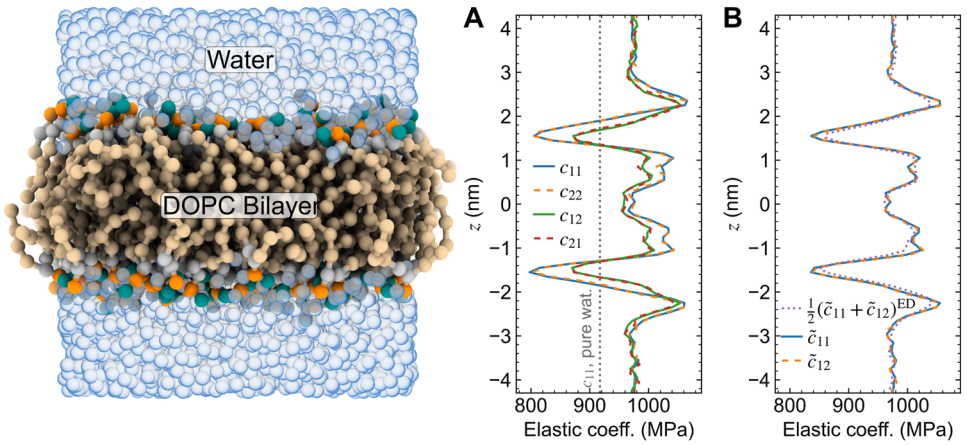

FIG. 5. Local elasticity profiles of a MARTINI DOPC lipid bilayer for coefficients that couple stress and strain in the x–y plane. (a) Coefficients c_{11}, c_{12}, c_{21}, and c_{22}. (b) Stress–strain coefficients $\tilde{c}_{11}$ and $\tilde{c}_{12}$ compared to the average obtained with the explicit deformation (ED) method. The dotted line in panel (a) shows the value obtained for pure MARTINI water (data from our companion paper[53]).

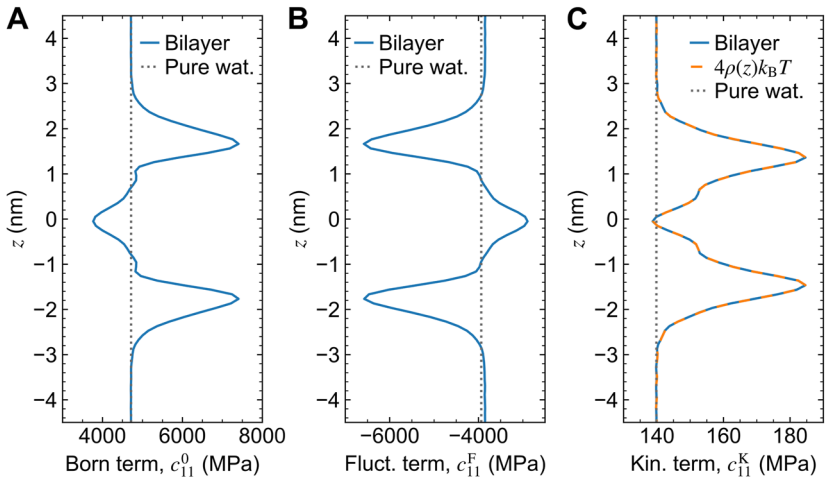

FIG. 6. Contributions from the Born [c_{11}^0, (a)], fluctuation [c_{11}^F, (b)], and kinetic [c_{11}^K, (c)] terms to the c_{11} coefficient for the DOPC lipid bilayer. Panel (c) includes a comparison to $4\rho(z)k_BT$, where $\rho(z)$ is the number density. This relation for c_{11}^K is obtained by integrating the momentum terms in Eq. (20d) using the equipartition theorem. Dotted lines show values obtained for pure MARTINI water (data from our companion paper[53]).

Continuing with the elastic coefficients that couple σ_{zz} and/or ϵ_{zz}, the expected symmetries due to lateral fluidity are conserved, as $c_{13}(z) = c_{23}(z)$ and $c_{31}(z) = c_{32}(z)$ [Fig. 7(a)]. However, the major symmetry between *xxzz* and *zzxx* components is again locally broken, as $c_{31}(z)$ remains constant due to mechanical equilibrium (see Sec. IV B), while $c_{13}(z)$ initially increases near the polar headgroups and significantly softens not only at the hydrocarbon–water interface but also in the acyl chain region [Fig. 7(a)]. As with the dodecane–water interface, the whole system major symmetry is maintained, as $\tilde{c}_{13}$ and $\tilde{c}_{31}$ have indistinguishable values. The coefficient $c_{33}(z)$ is also constant and matches the value of $c_{13}(z)$ in the water region, which is shifted to more positive values compared to $c_{31}(z)$ [Fig. 7(a)]. Furthermore, the elastic coefficients in the water region of the DOPC membrane are significantly larger in value compared to those of the pure liquid. Profiles of the stress–strain coefficients obtained with the explicit deformation method are also in excellent agreement with the SSF values [Fig. 7(b)].

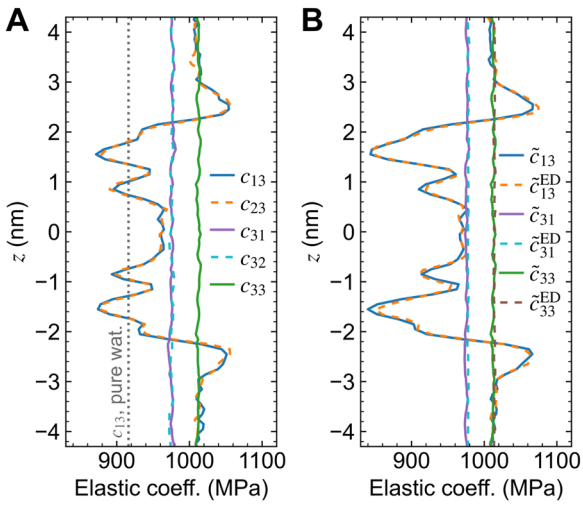

FIG. 7. Local elasticity profiles of a MARTINI DOPC lipid bilayer for coefficients that couple σ_{zz} and/or ϵ_{zz}. (a) Coefficients c_{13}, c_{23}, c_{31}, c_{32}, and c_{33}. (b) Stress–strain coefficients $\tilde{c}_{13}$, $\tilde{c}_{31}$, and $\tilde{c}_{13}$ compared to the explicit deformation (ED) method. The dotted line in panel (a) shows the value obtained for pure MARTINI water (data from our companion paper[53]).

D. Local shear moduli and membrane fluidity

The z-profiles for the shear elastic coefficients of the DOPC membrane are shown in Fig. 8. Similarly to the water–dodecane interface, the transverse shear coefficients $c_{44}(z)$ and $c_{55}(z)$ vanish [Fig. 8(a)], while the lateral shear coefficient $c_{66}(z)$ closely matches the transversely isotropic stability condition, $\frac{1}{2}[c_{11}(z) - c_{12}(z)] = c_{66}(z)$, and the negative of the lateral stress, $-\sigma_{xx}(z)$. Furthermore, the stress–strain transverse shear coefficient, $\tilde{c}_{44} = c_{44} + \frac{1}{2}(\sigma_{xx} + \sigma_{zz})$, is nonzero and is proportional to the stress, while the stress–strain lateral shear coefficient, $\tilde{c}_{66}$, vanishes [Fig. 8(b)]. The stress–strain transverse and lateral shear coefficients are also in excellent agreement with the profiles obtained from the explicit deformation method [Fig. 8(b)]. The observation that $\tilde{c}_{66}(z) = 0$ is also consistent with our earlier results, where $\tilde{c}_{11}(z) = \tilde{c}_{12}(z)$ [Fig. 5(b)]. See Sec. IV A for a discussion of why the stress–strain transverse shear coefficient $\tilde{c}_{44}^{ED}(z)$ is non-zero.

The stress–strain shear coefficients $\tilde{c}_{44}(z)$ and $\tilde{c}_{66}(z)$ are determined by the fluid nature of the lipid bilayer. The condition of lateral fluidity, associated with the lateral shear modulus $\lambda_S(z)$, can be cast as (i) a local constraint where $\lambda_S(z) = 0$ or (ii) a global constraint where $\int \lambda_S(z)dz = 0$.[13,15] Assuming that $\lambda_S(z) = \tilde{c}_{66}(z)$, our results indicate that the membrane is locally fluid as the lateral shear modulus vanishes across the bilayer, as has been proposed in previous works[13,30] (see also the more recent discussion by Pinigin *et al.*[16]). Beyond lateral movement, experimental and computational studies suggest that lipid tilt, defined as the average deviation of a lipid's orientation relative to the local membrane normal, plays an important role in defining the bilayer bending energy.[14–16,71,72,80–83] This elastic energy is characterized by the tilt modulus, κ_t, which is estimated to have values in the range of 40–100 mN/m ($10–24 k_BT/nm^2$) for PC membranes. Tilt–curvature theories[13–16] define the bilayer tilt modulus as the integral of the local transverse shear modulus, $\kappa_t = \int_{-\infty}^{\infty} \lambda_T(z)dz$. Following the work of Hamm and Kozlov[13]

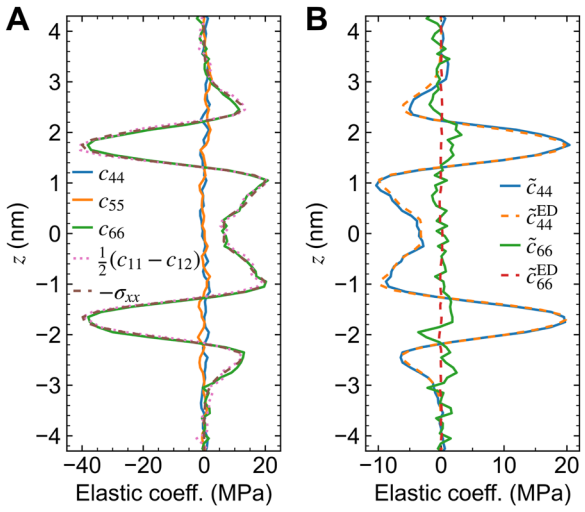

FIG. 8. Shear deformation elasticity profiles of a MARTINI DOPC lipid bilayer. (a) Coefficients c_{44} (y–z plane), c_{55} (x–z plane), and c_{66} (x–y plane). The negative of the lateral stress, $-\sigma_{xx}(z)$, is shown for comparison. (b) Stress–strain coefficients $\tilde{c}_{44}$ and $\tilde{c}_{66}$ compared to the explicit deformation (ED) method.

as well as Campelo *et al.*,[30] it would be natural to assume that the local transverse shear modulus corresponds to the stress–strain transverse shear coefficient, that is, $\lambda_T(z) = \tilde{c}_{44}(z)$, as this coefficient couples σ_{yz} to ϵ_{yz}. However, this poses a potential problem, given that the integral $\int_{-\infty}^{\infty} \tilde{c}_{44}(z)dz$ for the five independent simulation replicas varies between small positive and negative values and has an average value of $0.44 \pm 0.62 k_B T/\text{nm}^2$ indicating that the stress–strain transverse shear coefficient vanishes globally. This result does not necessarily mean that the tilt modulus is zero. It is possible that λ_T corresponds to some other combination of stress–strain coefficients. The coefficient $\tilde{c}_{44}(z)$ corresponds to a volume-preserving "simple shear" deformation in which the area and thickness of the bilayer remain constant. Therefore, the elastic energy of a tilted membrane, in which the area and thickness change, may require inclusion of additional terms beyond transverse shear. Furthermore, the broken symmetry between the coefficients $\tilde{c}_{13}(z)$ and $\tilde{c}_{31}(z)$ discussed in Sec. IV C may introduce additional nonisotropic energetic contributions related to tilt as discussed by Hamm and Kozlov.[13]

E. Membrane deformation moduli

As a lipid membrane is deformed, the individual elastic coefficients $\tilde{c}_{mn}(z)$ described in the previous sections give rise to different mechanical responses depending on the type of deformation. One of the most important membrane deformations to consider is lateral area stretching, which is macroscopically described by the area expansion modulus, K_A. As discussed in the Introduction, one can define the lateral stretch modulus profile,[13,30,31] $\lambda_L(z)$ [Eq. (1)], which is related to the global modulus through the relation $K_A = \int_{-\infty}^{\infty} \lambda_L(z)dz$. One can also define an approximate relation for the Young's modulus from the stress–strain elastic coefficients $\tilde{c}_{mn}(z)$,

$$\tilde{E}(z) \approx \frac{1}{2}[\tilde{c}_{11}(z) + \tilde{c}_{12}(z) + 2\tilde{c}_{33}(z) - 2\tilde{c}_{13}(z) - 2\tilde{c}_{31}(z)], \quad (39)$$

by assuming incompressibility, $\epsilon_{xx} + \epsilon_{yy} + \epsilon_{zz} = 0$, and grouping together all the free energy terms associated with area and thickness strains.[30] Under the constraint of incompressibility, the lateral stretch modulus is equivalent to the local Young's modulus, $\tilde{E}(z) = \lambda_L(z)$, and therefore these two quantities are used interchangeably in the literature.

Rather than grouping together like terms in the free energy, we take a continuum approach and define elastic moduli through the compliance tensor, s_{ijkl}, which relates strain to stress in the inverse of Hooke's law, $\epsilon_{ij} = s_{ijkl}\Delta\sigma_{kl}$. The individual compliance coefficients can be obtained from the elasticity tensor through

$$\tilde{c}_{ijkl}s_{klpq} = s_{ijkl}\tilde{c}_{klpq} = \frac{1}{2}(\delta_{ip}\delta_{jq} + \delta_{iq}\delta_{jp}), \quad (40)$$

or from the stiffness matrix in Voigt notation:

$$\tilde{c}_{mn}s_{np} = s_{mn}\tilde{c}_{np} = \delta_{mp}. \quad (41)$$

Note that the coefficients in s_{mn} are in general not equal to the corresponding s_{ijkl} because of the number of times a given s_{mn} appears in Eq. (41). However, they follow these simple relations:[62]

$$s_{ijkl} = s_{mn}, \quad \text{if } m,n = 1,2,3; \quad (42a)$$

$$s_{ijkl} = \frac{1}{2}s_{mn}, \quad \text{if } m = 1,2,3,\ n = 4,5,6, \text{ and if } m = 4,5,6,\ n = 1,2,3; \quad (42b)$$

$$s_{ijkl} = \frac{1}{4}s_{mn}, \quad \text{if } m,n = 4,5,6. \quad (42c)$$

Following the work of Scott,[84] we define the area modulus of a membrane, $\tilde{A}(z)$, as the ratio of an equibiaxial tension acting on the membrane plane (x–y) to the relative change in area on the same plane. As such, this modulus is given by the relation

$$\tilde{A}(z) = [s_{ijkl}(z)(\hat{x}_i\hat{x}_j + \hat{y}_i\hat{y}_j)(\hat{x}_k\hat{x}_l + \hat{y}_k\hat{y}_l)]^{-1}, \quad (43)$$

where $\{\hat{\boldsymbol{x}}, \hat{\boldsymbol{y}}, \hat{\boldsymbol{z}}\}$ are the orthonormal Cartesian unit vectors such that $\delta_{ij} = \hat{x}_i\hat{x}_j + \hat{y}_i\hat{y}_j + \hat{z}_i\hat{z}_j$. After substitution with the corresponding elements of the compliance, one obtains

$$\tilde{A}(z) = \frac{1}{2}(\tilde{c}_{11}(z) + \tilde{c}_{12}(z)) - \frac{\tilde{c}_{13}(z)\tilde{c}_{31}(z)}{\tilde{c}_{33}(z)}, \quad (44)$$

where we have assumed transverse isotropy, lateral fluidity, and only minor tensor symmetries. One can similarly define the elongation or Young's modulus for a membrane as the ratio of a uniaxial tension acting along $\hat{\boldsymbol{z}}$ relative to the change in extension in the same direction. This results in the following relation:

$$\tilde{E}(z) = [s_{ijkl}(z)\hat{z}_i\hat{z}_j\hat{z}_k\hat{z}_l]^{-1}, \quad (45)$$

$$= \tilde{c}_{33}(z) - \frac{2\tilde{c}_{13}(z)\tilde{c}_{31}(z)}{\tilde{c}_{11}(z) + \tilde{c}_{12}(z)}. \quad (46)$$

While $\tilde{A}(z)$ and $\tilde{E}(z)$ describe similar deformations, they need not be equal except in the limit of zero incompressibility (i.e., infinite bulk modulus).[84]

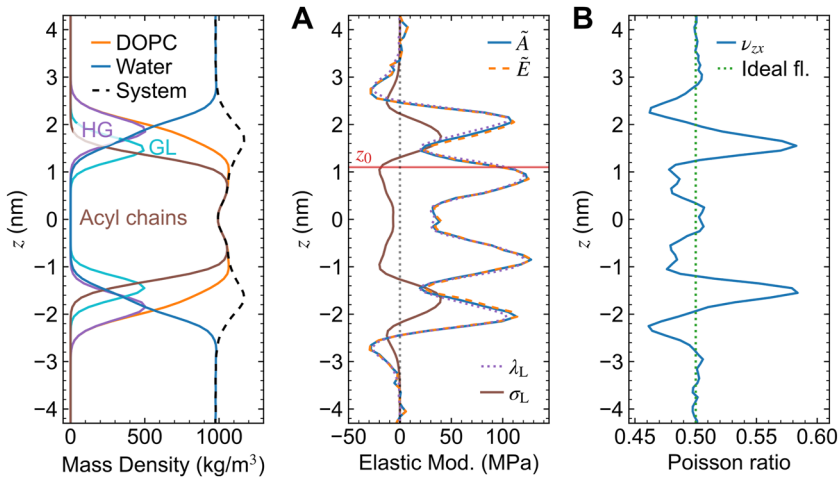

FIG. 9. Local elastic moduli of a MARTINI DOPC lipid bilayer. (a) Area, $\tilde{A}$, and Young's, $\tilde{E}$, moduli obtained from the coefficients $\tilde{c}_{mn}$ using Eqs. (44) and (46) compared to the lateral stretch modulus, λ_L, and lateral stress, σ_L. The position of the neutral surface, z_0, of the upper leaflet is shown in red. (b) Poisson ratio, ν_{zx}, describing the negative ratio of a strain induced in the x-direction, in the membrane plane, due to an applied strain in the z-direction, normal to the membrane [see Eq. (52)]. The inset on the left shows the mass density profiles of the DOPC lipids (HG = headgroups and GL = glycerol backbone), water molecules, and the entire system for reference.

Profiles for the $\tilde{A}(z)$, $\tilde{E}(z)$, and $\lambda_L(z)$ moduli for the DOPC membrane are shown in Fig. 9(a). The close agreement between $\tilde{A}(z)$ and $\lambda_L(z)$ shows that the definitions of these two quantities are consistent with each other. The combination of elastic coefficients that results in $\tilde{A}(z)$ gives rise to a unique variation pattern with maxima near the headgroup and acyl chain regions, and minima in the vicinity of the hydrocarbon–water interface and the bilayer midplane. Surprisingly, $\tilde{A}(z)$ displays negative values in the solvent region just beyond the headgroups indicating that this thin (~1 nm) layer of water softens the membrane's macroscopic elastic response. A local value of $\tilde{A}(z) < 0$, which implies that a pulling tension induces a local reduction in the area and not the expected expansion, does not violate the overall material stability conditions as long as $\int_{-\infty}^{\infty} \tilde{A}(z)dz > 0$. The area expansion modulus obtained by integrating $\tilde{A}(z)$ over the extent of the simulation box, $K_A = \int_{-\infty}^{\infty} \tilde{A}(z)dz$, has a value of 309 ± 12 mN/m $(72.2 \pm 2.7 k_B T/\text{nm}^2)$, which is in good agreement with the experimental range of 200–300 mN/m observed for PC lipids.[85–87] It is also in excellent agreement with the value of 309 ± 11 mN/m estimated from the area fluctuations in the *NPT* production simulation using the relation:

$$K_A^{\text{AF}} = \frac{k_B T \langle a \rangle}{\langle a^2 \rangle - \langle a \rangle^2}. \tag{47}$$

Beyond computing K_A, the area modulus can be used to estimate other important elastic properties, such as the position of the monolayer neutral surface,[30,31]

$$z_0 = \frac{\int_0^{\infty} \tilde{A}(z) z \, dz}{\int_0^{\infty} \tilde{A}(z) \, dz}. \tag{48}$$

Using this relation, we obtain a value of $z_0 = 1.10 \pm 0.03$ nm, which is located near the minima of the lateral stress profile below the glycerol backbone, as shown in Fig. 9(a). Wang and Deserno[88] determined the position of the pivotal plane, which coincides with the neutral surface for a planar membrane, for a DMPC MARTINI 2 system using the buckling method and obtained a value of 0.85 nm. While the two lipids have different lengths, DMPC has 3 CG tail beads instead of 4 for DOPC. The ratio of z_0 to the position of the maximum of the lateral stress profile for DMPC (in Wang and Deserno), $0.63 = \frac{0.85 \text{ nm}}{1.35 \text{ nm}}$, is in good agreement with our DOPC results, $0.65 = \frac{1.1 \text{ nm}}{1.7 \text{ nm}}$. Recently, Foley and Deserno[33] used the relation in Eq. (48) to estimate z_0 for the CG Cooke lipid model and found excellent agreement compared to values estimated from membrane curvature. We also estimated the position of the monolayer neutral surface using the spatial extent (SPEX) method[74,89] to analyze the fluctuations in a much larger DOPC membrane composed of 1800 lipids (see Methods). The value of z_0 obtained with the SPEX method, 0.912 ± 0.007, lies closer to the bilayer midplane compared to the value estimated from the area modulus.

Together with z_0, the area modulus $\tilde{A}(z)$ can be used to estimate the bending modulus, κ. Using the shorthand notation,

$$[\![X]\!]_n = \int_0^{\infty} (z - z_0)^n X(z) \, dz, \tag{49}$$

we can write an expression for the monolayer bending modulus based on the curvature–tilt theory of Terzi and Deserno[14,15] (TD):

$$\kappa_m = \overbrace{\underbrace{[\![\tilde{A}]\!]_2}^{\text{PKAG}} - [\![\sigma_L]\!]_2}^{\text{HK}} + [\![\lambda_s]\!]_2 \Big)^{\text{TD}}. \tag{50}$$

As we showed in Sec. IV D, the last term, $[\![\lambda_s]\!]_2$, vanishes as the lateral shear modulus is zero across the bilayer. Hamm and Kozlov[13] (HK) did not formally include this term in their theory but discussed how a nonzero lateral shear modulus would give rise to lipid "twist," as further discussed by TD.[14,15] Pinigin *et al.*[16] (PKAG) further argued that the $[\![\sigma_L]\!]_2$ term should also not be included in the estimation of the bending modulus based on stability conditions. The second moment of the area modulus has a value of $[\![\tilde{A}]\!]_2 = 8.1 \pm 2.6 \, k_B T$, which is in good agreement with the monolayer bending moduli 7.69 ± 0.05, 6.79 ± 0.05, and $7.6 \pm 0.1 k_B T$ obtained from power spectrum,[15,70] lipid director,[71–73] and SPEX[74] analyses

of the large 1800 DOPC membrane, respectively (see Methods for details). The addition of the second moment of the lateral stress profile term, $-[\![\sigma_L]\!]_2 = 2.25 \pm 0.15\ k_BT$, from Eq. (50), would result in an overestimation of the bending modulus compared to the values obtained with the other independent methods.

The small differences between the $\tilde{A}(z)$ and $\tilde{E}(z)$ profiles indicate that the membrane is not perfectly incompressible at the local level. We probe this through the Poisson ratio, which is defined as

$$\nu_{zx}(z) = -\tilde{E}(z)s_{ijkl}(z)\hat{z}_i\hat{z}_j\hat{x}_k\hat{x}_l, \tag{51}$$

$$= \frac{\tilde{c}_{31}(z)}{\tilde{c}_{11}(z) + \tilde{c}_{12}(z)}. \tag{52}$$

Here, $\hat{\boldsymbol{z}}$ defines the direction of extension (i.e., the direction of the applied force) and $\hat{\boldsymbol{x}}$ the direction of transverse deformation. The local Poisson ratio for the DOPC membrane has values near 0.5 in the "bulk" solvent region and near the bilayer midplane [Fig. 9(b)], yet it deviates from the ideal incompressible fluid behavior ($\nu_{zx} = 0.5$) throughout the depth of the membrane. Values greater than 0.5 are observed in the headgroup region, whereas values less than 0.5 are observed around the acyl chains and in the region of water just above the headgroups. These variations balance each other out such that the average value of ν_{zx} for the entire system is 0.501. To understand the physical meaning of the local Poisson ratio, consider that when a normal compression induces a lateral expansion, the local volume can (i) decrease for $\nu_{zx}(z) < 0.5$, (ii) remain constant for $\nu_{zx}(z) = 0.5$, or (iii) increase for $\nu_{zx}(z) > 0.5$.[90] A similar local Poisson ratio was obtained for a MARTINI 3 DMPC membrane using the explicit deformation method and assuming global incompressibility.[34] Note that while the Poisson ratio of isotropic materials is bound by $-1 < \nu < 0.5$ due to the material stability conditions, the Poisson ratios of transversely isotropic and other anisotropic materials are not bounded.[91] Terzi *et al.*[92] obtained the local Poisson ratio for an atomistic DOPC membrane via a volumetric approach and similarly observed values less than 0.5 in the acyl chain region and greater than 0.5 near the headgroups. While the Poisson ratio in our MARTINI DOPC analysis reaches maximum values ~0.58 compared to ~0.52 in the atomistic DOPC, it is not clear whether these small differences are due to assumptions made in their analysis regarding the symmetry of the elasticity tensor and/or properties of the coarse-grained vs atomistic simulations.

We end this section by exploring the bulk modulus, $\tilde{B}(z)$. This is defined as the ratio of the hydrostatic stress to the relative change in volume and is given by the following relation:

$$\tilde{B}(z) = [s_{ijkl}(z)(\hat{x}_i\hat{x}_j + \hat{y}_i\hat{y}_j + \hat{z}_i\hat{z}_j)(\hat{x}_k\hat{x}_l + \hat{y}_k\hat{y}_l + \hat{z}_k\hat{z}_l)]^{-1}, \tag{53}$$

$$= \frac{\tilde{c}_{11}(z)\tilde{c}_{33}(z) + \tilde{c}_{12}(z)\tilde{c}_{33}(z) - 2\tilde{c}_{13}(z)\tilde{c}_{31}(z)}{\tilde{c}_{11}(z) + \tilde{c}_{12}(z) + 2\tilde{c}_{33}(z) - 2\tilde{c}_{13}(z) - 2\tilde{c}_{31}(z)}. \tag{54}$$

The bulk modulus profile, $\tilde{B}(z)$, for the DOPC bilayer is shown in Fig. S2A. Unlike the area and Young's moduli, $\tilde{B}(z)$ has many singularities near the headgroup and water regions, which are due to the denominator in Eq. (54) approaching values near zero (Fig. S2B). Despite these local singularities, the bulk modulus for the entire system is well defined and has a value of $K_V = 975 \pm 1$ MPa, obtained from Eq. (54) using the average values of the individual stress–strain coefficients. The system bulk modulus is in excellent agreement with the value obtained from volume fluctuations in the *NPT* simulation, $K_V^{AF} = 981 \pm 7$ MPa, using the following formula:

$$K_V^{AF} = \frac{k_BT\langle V\rangle}{\langle V^2\rangle - \langle V\rangle^2}. \tag{55}$$

Note that these two values are for the entire system and not just for the membrane. One could extract the bulk modulus for the bilayer from that of the system by assuming that the moduli of the water and bilayer behave as two springs in series,[92] but our earlier results, showing that the elastic coefficients in the water region can be significantly different from those of the bulk liquid due to the stress fluctuations, do not support this physics analogy. Early experiments for DPPC (1,2-dipalmitoyl-sn-glycero-3-phosphocholine) in multilamellar vesicles in the fluid phase (320 K) obtained a bulk modulus value of 1300 MPa. Terzi *et al.*[92] analyzed various experimental and all-atom simulation data to obtain bilayer bulk modulus values in the range of 600–2000 MPa.

V. CONCLUSIONS

We have presented an extensive characterization of the local elastic properties of a simple liquid–liquid interface and a lipid membrane using the SSF method. The excellent agreement with results obtained from the independent explicit deformation method demonstrates the robustness of the local SSF formula and its applicability for soft materials. The unexpected breaking of the local major symmetry of the elasticity tensor for both the water–dodecane interface and the DOPC membrane must be carefully considered when defining deformation moduli from the individual coefficients. Our results shed light on important questions and assumptions regarding membrane fluidity and incompressibility that have been present in the literature for the last couple of decades. The finding that the lateral shear stress–strain coefficient $\tilde{c}_{66}(z)$ of the DOPC membrane is zero throughout the bilayer questions the notion that simple shear in the plane of the membrane contributes to the elastic deformation energy as proposed by tilt–curvature theories.[13–15] Similarly, the transverse shear stress–strain coefficient $\tilde{c}_{66}(z)$ for the DOPC membrane is locally nonzero, but its integral vanishes. This does not necessarily mean that there is no energetic penalty associated with lipid tilt, but it suggests that simple transverse shear (i.e., volume- and area-preserving) does not contribute to the tilt modulus, and therefore its microscopic definition may need to be reconsidered in tilt–curvature theories.[13–16] By objectively defining the area, Young's, and bulk moduli as well as the Poisson ratio through the compliance tensor, we have directly probed the assumption of membrane incompressibility. The local Poisson ratio for the DOPC membrane shows that the bilayer can significantly deviate locally from the ideal incompressible behavior, yet the area and Young's moduli are largely indistinguishable, which suggests that the assumption of membrane incompressibility is a viable approximation under certain circumstances.

SUPPLEMENTARY MATERIAL

See the supplementary material for additional figures including elastic coefficients, area modulus, and Poisson ratio for the smaller

128-lipid DOPC bilayer, as well as the bulk modulus profile of the 200-lipid DOPC bilayer.

ACKNOWLEDGMENTS

J.M.V. and A.L.L. acknowledge the support of the National Science Foundation through Grant No. CHE-1944892/2326678. Computations were performed, in part, on the Vermont Advanced Computing Core, supported in part by NSF Award No. OAC-1827314. This work also used the NCSA Delta supercomputer at the University of Illinois at Urbana-Champaign through Allocation No. BIO240313 from the Advanced Cyberinfrastructure Coordination Ecosystem: Services & Support (ACCESS) program, which is supported by U.S. National Science Foundation Grant Nos. 2138259, 2138286, 2138307, 2137603, and 2138296. We thank Muhammed Ergüder and Markus Deserno for assistance with the power spectra and lipid director analysis code.

AUTHOR DECLARATIONS

Conflict of Interest

The authors have no conflicts to disclose.

Author Contributions

Andrew L. Lewis: Conceptualization (equal); Data curation (equal); Formal analysis (equal); Investigation (equal); Methodology (equal); Software (equal); Visualization (equal); Writing – original draft (equal); Writing – review & editing (equal). **Benjamin Himberg**: Data curation (equal); Investigation (equal); Methodology (equal); Software (equal); Visualization (supporting). **Alejandro Torres-Sánchez**: Conceptualization (equal); Methodology (equal); Software (equal); Writing – review & editing (equal). **Juan M. Vanegas**: Conceptualization (lead); Data curation (equal); Formal analysis (equal); Funding acquisition (lead); Investigation (lead); Methodology (equal); Resources (lead); Software (equal); Supervision (lead); Validation (equal); Visualization (equal); Writing – original draft (lead); Writing – review & editing (equal).

DATA AVAILABILITY

The data that support the findings of this study are available from the corresponding author upon reasonable request. The custom GROMACS-LS and MDStress library codes are available from the project website at https://github.com/vanegasj/gromacs-ls and have also been deposited in the Zenodo repository.[54]

REFERENCES

[1]H. T. McMahon and J. L. Gallop, "Membrane curvature and mechanisms of dynamic cell membrane remodelling," Nature **438**, 590–596 (2005).
[2]L. V. Chernomordik and M. M. Kozlov, "Mechanics of membrane fusion," Nat. Struct. Mol. Biol. **15**, 675–683 (2008).
[3]R. Behnia and S. Munro, "Organelle identity and the signposts for membrane traffic," Nature **438**, 597–604 (2005).
[4]M. M. Kozlov, F. Campelo, N. Liska, L. V. Chernomordik, S. J. Marrink, and H. T. McMahon, "Mechanisms shaping cell membranes," Curr. Opin. Cell Biol. **29**, 53–60 (2014).
[5]H. T. McMahon and E. Boucrot, "Membrane curvature at a glance," J. Cell Sci. **128**, 1065–1070 (2015).
[6]P. Bassereau, R. Jin, T. Baumgart, M. Deserno, R. Dimova, V. A. Frolov, P. V. Bashkirov, H. Grubmüller, R. Jahn, H. J. Risselada, L. Johannes, M. M. Kozlov, R. Lipowsky, T. J. Pucadyil, W. F. Zeno, J. C. Stachowiak, D. Stamou, A. Breuer, L. Lauritsen, C. Simon, C. Sykes, G. A. Voth, and T. R. Weikl, "The 2018 biomembrane curvature and remodeling roadmap," J. Phys. D: Appl. Phys. **51**, 343001 (2018).
[7]P. B. Canham, "The minimum energy of bending as a possible explanation of the biconcave shape of the human red blood cell," J. Theor. Biol. **26**, 61–81 (1970).
[8]W. Helfrich, "Elastic properties of lipid bilayers: Theory and possible experiments," Z. Naturforsch., C **28**, 693–703 (1973).
[9]E. A. Evans, "Bending resistance and chemically induced moments in membrane bilayers," Biophys. J. **14**, 923–931 (1974).
[10]M. M. Kozlov, S. L. Leikin, and V. S. Markin, "Elastic properties of interfaces. Elasticity moduli and spontaneous geometric characteristics," J. Chem. Soc., Faraday Trans. 2 **85**(4), 277–292 (1989).
[11]M. M. Kozlov and M. Winterhalter, "Elastic moduli for strongly curved monoplayers. Position of the neutral surface," J. Phys. II Fr. **1**, 1077–1084 (1991).
[12]L. D. Landau, L. P. Pitaevskii, E. M. Lifshitz, and A. M. Kosevich, *Theory of Elasticity*, 3rd ed. (Elsevier Butterworth-Heinemann, New York, 1986), Vol. VII.
[13]M. Hamm and M. M. Kozlov, "Elastic energy of tilt and bending of fluid membranes," Eur. Phys. J. E **3**, 323–335 (2000).
[14]M. M. Terzi and M. Deserno, "Novel tilt-curvature coupling in lipid membranes," J. Chem. Phys. **147**, 084702 (2017).
[15]M. M. Terzi, M. F. Ergüder, and M. Deserno, "A consistent quadratic curvature-tilt theory for fluid lipid membranes," J. Chem. Phys. **151**, 164108 (2019).
[16]K. V. Pinigin, P. I. Kuzmin, S. A. Akimov, and T. R. Galimzyanov, "Additional contributions to elastic energy of lipid membranes: Tilt-curvature coupling and curvature gradient," Phys. Rev. E **102**, 042406 (2020).
[17]E. Lindahl and O. Edholm, "Spatial and energetic-entropic decomposition of surface tension in lipid bilayers from molecular dynamics simulations," J. Chem. Phys. **113**, 3882–3893 (2000).
[18]J. Sonne, F. Y. Hansen, and G. H. Peters, "Methodological problems in pressure profile calculations for lipid bilayers," J. Chem. Phys. **122**, 124903 (2005).
[19]O. H. S. Ollila, T. Róg, M. Karttunen, and I. Vattulainen, "Role of sterol type on lateral pressure profiles of lipid membranes affecting membrane protein functionality: Comparison between cholesterol, desmosterol, 7-dehydrocholesterol and ketosterol," J. Struct. Biol. **159**, 311–323 (2007).
[20]O. H. S. Ollila, H. J. Risselada, M. Louhivuori, E. Lindahl, I. Vattulainen, and S. J. Marrink, "3D pressure field in lipid membranes and membrane-protein complexes," Phys. Rev. Lett. **102**, 078101 (2009).
[21]J. M. Vanegas, A. Torres-Sánchez, and M. Arroyo, "Importance of force decomposition for local stress calculations in biomembrane molecular simulations," J. Chem. Theory Comput. **10**, 691–702 (2014).
[22]A. Torres-Sánchez, J. M. Vanegas, and M. Arroyo, "Examining the mechanical equilibrium of microscopic stresses in molecular simulations," Phys. Rev. Lett. **114**, 258102 (2015).
[23]A. J. Sodt, R. M. Venable, E. Lyman, and R. W. Pastor, "Nonadditive compositional curvature energetics of lipid bilayers," Phys. Rev. Lett. **117**, 138104 (2016).
[24]C. M. Winkeljohn, B. Himberg, and J. M. Vanegas, "Balance of solvent and chain interactions determines the local stress state of simulated membranes," J. Phys. Chem. B **124**, 6963–6971 (2020).
[25]J. H. Irving and J. G. Kirkwood, "The statistical mechanical theory of transport processes. IV. The equations of hydrodynamics," J. Chem. Phys. **18**, 817–829 (1950).
[26]W. Noll, "Die Herleitung der Grundgleichungen der Thermomechanik der Kontinua aus der Statistischen Mechanik," Indiana Univ. Math. J. **4**, 627–646 (1955).
[27]R. B. Lehoucq and A. Von Lilienfeld-Toal, "Translation of Walter Noll's 'Derivation of the fundamental equations of continuum thermodynamics from statistical mechanics,'" J. Elasticity **100**, 5–24 (2010).
[28]R. J. Hardy, "Formulas for determining local properties in molecular-dynamics simulations: Shock waves," J. Chem. Phys. **76**, 622–628 (1982).

[29]N. C. Admal and E. B. Tadmor, "A unified interpretation of stress in molecular systems," J. Elasticity **100**, 63–143 (2010).
[30]F. Campelo, C. Arnarez, S. J. Marrink, and M. M. Kozlov, "Helfrich model of membrane bending: From Gibbs theory of liquid interfaces to membranes as thick anisotropic elastic layers," Adv. Colloid Interface Sci. **208**, 25–33 (2014).
[31]S. L. Foley and M. Deserno, "Chapter three - Quantifying uncertainty in transmembrane stresses and moments in simulation," in *Biophysical Approaches for the Study of Membrane Structure—Part B: Theory and Simulations*, *Methods in Enzymology*, edited by M. Deserno and T. Baumgart (Academic Press, 2024), Vol. 701, pp. 83–122.
[32]S. J. Marrink, H. J. Risselada, S. Yefimov, D. P. Tieleman, and A. H. de Vries, "The MARTINI force field: Coarse grained model for biomolecular simulations," J. Phys. Chem. B **111**, 7812–7824 (2007).
[33]S. L. Foley and M. Deserno, "Asymmetric membrane 'sticky tape' enables simultaneous relaxation of area and curvature in simulation," J. Chem. Phys. **160**, 064111 (2024).
[34]M. A. Kalutskii, T. R. Galimzyanov, and K. V. Pinigin, "Determination of elastic parameters of lipid membranes from simulation under varied external pressure," Phys. Rev. E **107**, 024414 (2023).
[35]J. F. Lutsko, "Stress and elastic constants in anisotropic solids: Molecular dynamics techniques," J. Appl. Phys. **64**, 1152–1154 (1988).
[36]J. F. Lutsko, "Generalized expressions for the calculation of elastic constants by computer simulation," J. Appl. Phys. **65**, 2991–2997 (1989).
[37]A. A. Gusev, M. M. Zehnder, and U. W. Suter, "Fluctuation formula for elastic constants," Phys. Rev. B **54**, 1–4 (1996).
[38]D. Lips and P. Maass, "Stress-stress fluctuation formula for elastic constants in the *NPT* ensemble," Phys. Rev. E **97**, 053002 (2018).
[39]M. Born and K. Huang, *Dynamical Theory of Crystal Lattices* (Oxford University Press, 1954).
[40]K. Huang, "On the atomic theory of elasticity," Proc. R. Soc. A **203**, 178–194 (1950).
[41]T. H. K. Barron and M. L. Klein, "Second-order elastic constants of a solid under stress," Proc. Phys. Soc. **85**, 523–532 (1965).
[42]F. Bavaud, P. Choquard, and J. R. Fontaine, "Statistical mechanics of elastic moduli," J. Stat. Phys. **42**, 621–646 (1986).
[43]E. B. Tadmor and R. E. Miller, *Modeling Materials: Continuum, Atomistic, and Multiscale Techniques* (Cambridge University Press, Cambridge; New York, 2011).
[44]K. Van Workum, G. Gao, J. D. Schall, and J. A. Harrison, "Expressions for the stress and elasticity tensors for angle-dependent potentials," J. Chem. Phys. **125**, 144506 (2006).
[45]J. Grießer, L. Frérot, J. A. Oldenstaedt, M. H. Müser, and L. Pastewka, "Analytic elastic coefficients in molecular calculations: Finite strain, nonaffine displacements, and many-body interatomic potentials," Phys. Rev. Mater. **7**, 073603 (2023).
[46]A. Torres-Sánchez, J. M. Vanegas, and M. Arroyo, "Geometric derivation of the microscopic stress: A covariant central force decomposition," J. Mech. Phys. Solids **93**, 224–239 (2016).
[47]D. R. Squire, A. C. Holt, and W. G. Hoover, "Isothermal elastic constants for argon. Theory and Monte Carlo calculations," Physica **42**, 388–397 (1969).
[48]K. Van Workum, K. Yoshimoto, J. de Pablo, and J. Douglas, "Isothermal stress and elasticity tensors for ions and point dipoles using Ewald summations," Phys. Rev. E **71**, 061102 (2005).
[49]H. Xu, J. P. Wittmer, P. Polińska, and J. Baschnagel, "Impulsive correction to the elastic moduli obtained using the stress-fluctuation formalism in systems with truncated pair potential," Phys. Rev. E **86**, 046705 (2012).
[50]J. P. Wittmer, H. Xu, P. Polińska, F. Weysser, and J. Baschnagel, "Shear modulus of simulated glass-forming model systems: Effects of boundary condition, temperature, and sampling time," J. Chem. Phys. **138**, 12A533 (2013).
[51]O. Lenz and F. Schmid, "A simple computer model for liquid lipid bilayers," J. Mol. Liq. **117**, 147–152 (2005).
[52]O. Lenz and F. Schmid, "Structure of symmetric and asymmetric "Ripple" phases in lipid bilayers," Phys. Rev. Lett. **98**, 058104 (2007).
[53]A. L. Lewis, B. Himberg, A. Torres-Sánchez, and J. M. Vanegas, "Microscopic elasticity from MD. I. Bulk solid and fluid systems," J. Chem. Phys. **164**, 014110 (2025).
[54]J. M. Vanegas, B. Himberg, A. Lewis, and A. Torres-Sánchez (2025). "GROMACS-LS and MDStress library: Tools for local stress and elasticity calculations," Zenodo. https://zenodo.org/records/17179200
[55]T. C. Doyle and J. L. Ericksen, "Nonlinear elasticity," in *Advances in Applied Mechanics IV*, edited by H. L. Dryden and Th. von Kármán (Elsevier, 1956), Vol. 4, pp. 53–115.
[56]J. Marsden and T. J. R. Hughes, *Mathematical Foundations of Elasticity* (Dover Publications, Inc., New York, 1983).
[57]J. C. Simo and J. E. Marsden, "On the rotated stress tensor and the material version of the Doyle-Ericksen formula," Arch. Ration. Mech. Anal. **86**, 213–231 (1984).
[58]L. Mistura, "The pressure tensor in nonuniform fluids," J. Chem. Phys. **83**, 3633–3637 (1985).
[59]L. Mistura, "The definition of the pressure tensor in the statistical mechanics of nonuniform classical fluids," Int. J. Thermophys. **8**, 397–403 (1987).
[60]F. D. Murnaghan, "Finite deformations of an elastic solid," Am. J. Math. **59**, 235–260 (1937).
[61]D. C. Wallace, "Thermoelasticity of stressed materials and comparison of various elastic constants," Phys. Rev. **162**, 776–789 (1967).
[62]D. C. Wallace, *Thermodynamics of Crystals* (John Wiley & Sons, Inc., New York, 1972).
[63]F. Birch, "Finite elastic strain of cubic crystals," Phys. Rev. **71**, 809–824 (1947).
[64]M. J. Abraham, T. Murtola, R. Schulz, S. Páll, J. C. Smith, B. Hess, and E. Lindahl, "GROMACS: High performance molecular simulations through multi-level parallelism from laptops to supercomputers," SoftwareX **1-2**, 19–25 (2015).
[65]P. C. T. Souza, R. Alessandri, J. Barnoud, S. Thallmair, I. Faustino, F. Grünewald, I. Patmanidis, H. Abdizadeh, B. M. H. Bruininks, T. A. Wassenaar, P. C. Kroon, J. Melcr, V. Nieto, V. Corradi, H. M. Khan, J. Domański, M. Javanainen, H. Martinez-Seara, N. Reuter, R. B. Best, I. Vattulainen, L. Monticelli, X. Periole, D. P. Tieleman, A. H. de Vries, and S. J. Marrink, "MARTINI 3: A general purpose force field for coarse-grained molecular dynamics," Nat. Methods **18**, 382–388 (2021).
[66]G. Bussi, D. Donadio, and M. Parrinello, "Canonical sampling through velocity rescaling," J. Chem. Phys. **126**, 014101 (2007).
[67]M. Bernetti and G. Bussi, "Pressure control using stochastic cell rescaling," J. Chem. Phys. **153**, 114107 (2020).
[68]H. Kim, B. Fábián, and G. Hummer, "Neighbor list artifacts in molecular dynamics simulations," J. Chem. Theory Comput. **19**, 8919–8929 (2023).
[69]T. A. Wassenaar, H. I. Ingólfsson, R. A. Böckmann, D. P. Tieleman , and S. J. Marrink, "Computational lipidomics with insane: A versatile tool for generating custom membranes for molecular simulations," J. Chem. Theory Comput. **11**, 2144–2155 (2015).
[70]M. F. Ergüder and M. Deserno, "Identifying systematic errors in a power spectral analysis of simulated lipid membranes," J. Chem. Phys. **154**, 214103 (2021).
[71]M. C. Watson, E. S. Penev, P. M. Welch, and F. L. H. Brown, "Thermal fluctuations in shape, thickness, and molecular orientation in lipid bilayers," J. Chem. Phys. **135**, 244701 (2011).
[72]M. C. Watson, E. G. Brandt, P. M. Welch, and F. L. H. Brown, "Determining biomembrane bending rigidities from simulations of modest size," Phys. Rev. Lett. **109**, 028102 (2012).
[73]Z. A. Levine, R. M. Venable, M. C. Watson, M. G. Lerner, J.-E. Shea, R. W. Pastor, and F. L. H. Brown, "Determination of biomembrane bending moduli in fully atomistic simulations," J. Am. Chem. Soc. **136**, 13582–13585 (2014).
[74]K. C. Sapp, A. H. Beaven, and A. J. Sodt, "Spatial extent of a single lipid's influence on bilayer mechanics," Phys. Rev. E **103**, 042413 (2021).
[75]C. R. Harris, K. J. Millman, S. J. van der Walt, R. Gommers, P. Virtanen, D. Cournapeau, E. Wieser, J. Taylor, S. Berg, N. J. Smith, R. Kern, M. Picus, S. Hoyer, M. H. van Kerkwijk, M. Brett, A. Haldane, J. F. del Río, M. Wiebe, P. Peterson, P. Gérard-Marchant, K. Sheppard, T. Reddy, W. Weckesser, H. Abbasi, C. Gohlke, and T. E. Oliphant, "Array programming with NumPy," Nature **585**, 357–362 (2020).

[76]P. Virtanen, R. Gommers, T. E. Oliphant, M. Haberland, T. Reddy, D. Cournapeau, E. Burovski, P. Peterson, W. Weckesser, J. Bright, S. J. van der Walt, M. Brett, J. Wilson, K. J. Millman, N. Mayorov, A. R. J. Nelson, E. Jones, R. Kern, E. Larson, C. J. Carey, İ. Polat, Y. Feng, E. W. Moore, J. VanderPlas, D. Laxalde, J. Perktold, R. Cimrman, I. Henriksen, E. A. Quintero, C. R. Harris, A. M. Archibald, A. H. Ribeiro, F. Pedregosa, P. van Mulbregt, A. Vijaykumar *et al.*, "SciPy 1.0: Fundamental algorithms for scientific computing in python," Nat. Methods **17**, 261–272 (2020).
[77]J. D. Hunter, "Matplotlib: A 2D graphics environment," Comput. Sci. Eng. **9**, 90–95 (2007).
[78]A. R. Braun, E. G. Brandt, O. Edholm, J. F. Nagle, and J. N. Sachs, "Determination of electron density profiles and area from simulations of undulating membranes," Biophys. J. **100**, 2112–2120 (2011).
[79]M. Hu, J. J. Briguglio, and M. Deserno, "Determining the Gaussian curvature modulus of lipid membranes in simulations," Biophys. J. **102**, 1403–1410 (2012).
[80]E. R. May, A. Narang, and D. I. Kopelevich, "Role of molecular tilt in thermal fluctuations of lipid membranes," Phys. Rev. E **76**, 021913 (2007).
[81]M. S. Jablin, K. Akabori, and J. F. Nagle, "Experimental support for tilt-dependent theory of biomembrane mechanics," Phys. Rev. Lett. **113**, 248102 (2014).
[82]J. F. Nagle, M. S. Jablin, S. Tristram-Nagle, and K. Akabori, "What are the true values of the bending modulus of simple lipid bilayers?," Chem. Phys. Lipids **185**, 3–10 (2015).
[83]J. F. Nagle, "Experimentally determined tilt and bending moduli of single-component lipid bilayers," Chem. Phys. Lipids **205**, 18–24 (2017).
[84]N. H. Scott, "An area modulus of elasticity: Definition and properties," J. Elasticity **58**, 269–275 (2000).
[85]W. Rawicz, K. C. Olbrich, T. McIntosh, D. Needham, and E. Evans, "Effect of chain length and unsaturation on elasticity of lipid bilayers," Biophys. J. **79**, 328–339 (2000).
[86]W. Rawicz, B. A. Smith, T. J. McIntosh, S. A. Simon, and E. Evans, "Elasticity, strength, and water permeability of bilayers that contain raft microdomain-forming lipids," Biophys. J. **94**, 4725–4736 (2008).
[87]J. R. Henriksen and J. H. Ipsen, "Measurement of membrane elasticity by micropipette aspiration," Eur. Phys. J. E **14**, 149–167 (2004).
[88]X. Wang and M. Deserno, "Determining the lipid tilt modulus by simulating membrane buckles," J. Phys. Chem. B **120**, 6061–6073 (2016).
[89]A. Hossein, K. Sapp, and A. Sodt, "Chapter fourteen - Computing the influence of lipids and lipid complexes on membrane mechanics," in *Methods in Enzymology, Biophysical Approaches for the Study of Membrane Structure—Part B: Theory and Simulations*, edited by M. Deserno and T. Baumgart (Academic Press, 2024), Vol. 701, pp. 515–540.
[90]I. Pajic-Lijakovic, M. Milivojevic, and P. V. E. McClintock, "Compressibility of biological systems: The viscoelastic Poisson's ratio," Adv. Phys.: X **10**, 2440023 (2025).
[91]T. C. T. Ting and T. Chen, "Poisson's ratio for anisotropic elastic materials can have no bounds," Q. J. Mech. Appl. Math. **58**, 73–82 (2005).
[92]M. M. Terzi, M. Deserno, and J. F. Nagle, "Mechanical properties of lipid bilayers: A note on the Poisson ratio," Soft Matter **15**, 9085–9092 (2019).

SUPPLEMENTARY MATERIAL
Microscopic elasticity from MD part II: Liquid interfaces and lipid membranes

Andrew L. Lewis
Department of Physics, The University of Vermont, Burlington, VT, USA.

Benjamin Himberg
Materials Science Graduate Program, The University of Vermont, Burlington, VT, USA.

Alejandro Torres-Sánchez
European Molecular Biology Laboratory, Barcelona, Spain.

Juan M. Vanegas*
Department of Biochemistry and Biophysics, Oregon State University, Corvallis, OR, USA.
(Dated: December 5, 2025)

* vanegasj@oregonstate.edu

I. SUPPLEMENTARY FIGURES

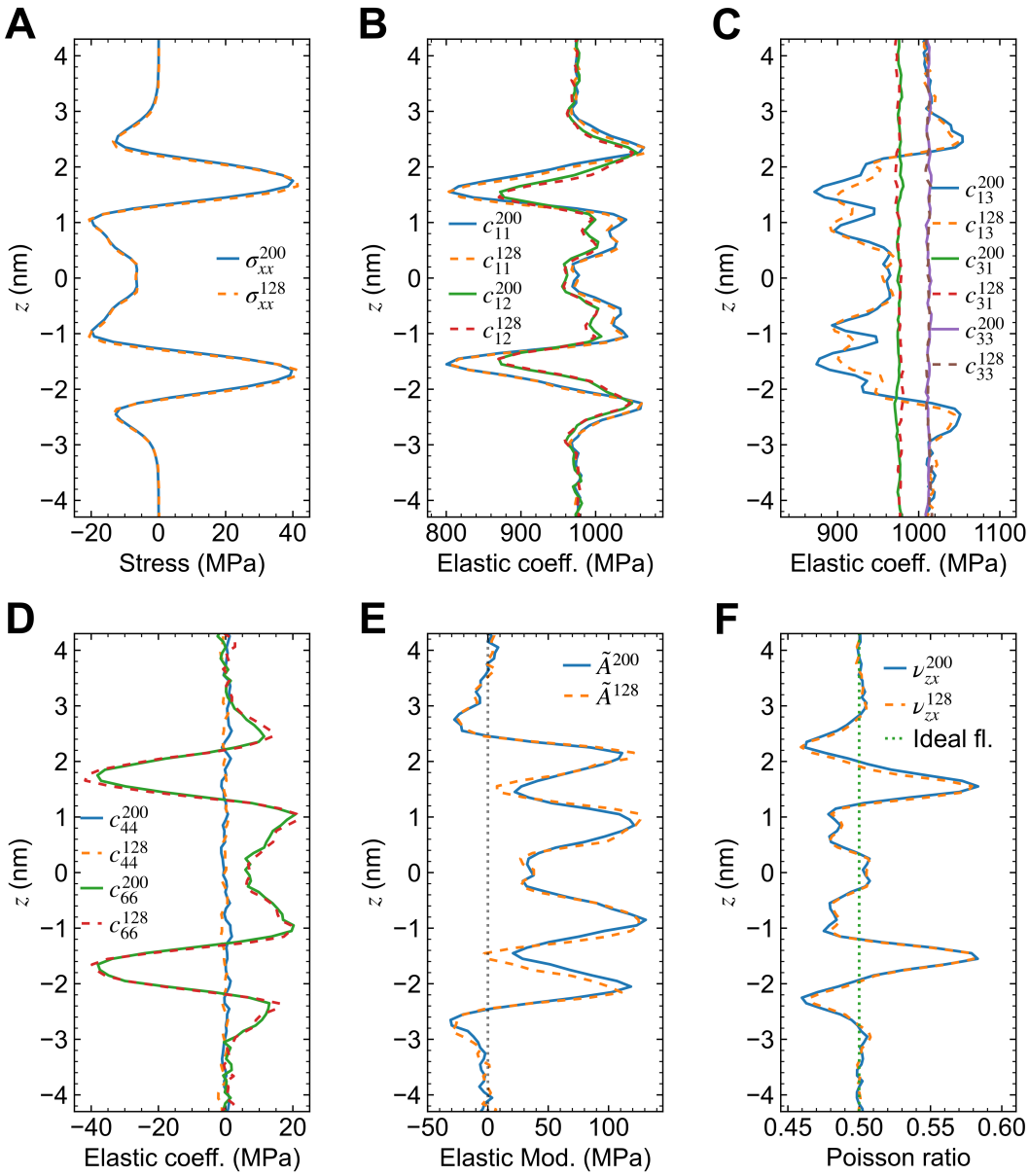

FIG. S1. Effects of system size on the local stress and elasticity profiles of MARTINI DOPC bilayers composed of 128 and 200 lipids (with equal water/lipid ratios). A) Lateral stress, σ_{xx}. B) Coefficients that couple stress and strain in the $x-y$ plane, c_{11}, c_{12}, c_{21}, and c_{22}. C) Coefficients that couple σ_{zz} and/or ϵ_{zz}, c_{13}, c_{23}, c_{31}, c_{32}. D) Transverse and lateral shear coefficients, c_{44} and c_{66}. E) Area modulus, $\tilde{A}$. F) Poisson ratio, ν_{zx}.

$$\tilde{B} = \frac{\tilde{c}_{11}\tilde{c}_{33} + \tilde{c}_{12}\tilde{c}_{33} - 2\tilde{c}_{13}\tilde{c}_{31}}{\tilde{c}_{11} + \tilde{c}_{12} + 2\tilde{c}_{33} - 2\tilde{c}_{13} - 2\tilde{c}_{31}} = \tilde{c}_{33}\left(\frac{1 - \frac{2\tilde{c}_{13}\tilde{c}_{31}}{\tilde{c}_{33}(\tilde{c}_{11}+\tilde{c}_{12})}}{1 + \frac{2(\tilde{c}_{33}-\tilde{c}_{13}-\tilde{c}_{31})}{\tilde{c}_{11}+\tilde{c}_{12}}}\right)$$

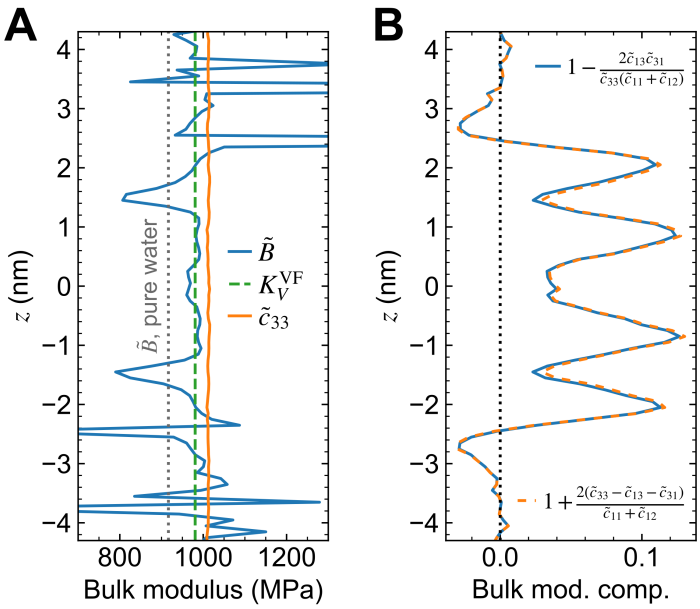

FIG. S2. A) Local bulk modulus, $\tilde{B}(z)$, of a MARTINI DOPC bilayer (200 lipids) compared to the global bulk modulus of the entire system obtained from volume fluctuations, K_V^{VF}, the bulk modulus of pure water (dotted gray line) and the stress-strain coefficient $\tilde{c}_{33}$. B) Components of the bulk modulus formula (see inset above) show that singularities in $\tilde{B}(z)$ in the headgroup and water regions correspond to points where the denominator approaches values near zero.